HHS Public Access

Author manuscript

Cell Rep. Author manuscript; available in PMC 2021 November 27.

Published in final edited form as:

Cell Rep. 2021 November 02; 37(5): 109905. doi:10.1016/j.celrep.2021.109905.

FARP1, ARHGEF39, and TIAM2 are essential receptor tyrosine kinase effectors for Rac1-dependent cell motility in human lung adenocarcinoma

Mariana Cooke[1,2], **Gabriel Kreider-Letterman**[3], **Martin J. Baker**[1], **Suli Zhang**[1], **Neil T. Sullivan**[4], **Evgeniy Eruslanov**[4], **Martin C. Abba**[5], **Silvia M. Goicoechea**[3], **Rafael García-Mata**[3,*], **Marcelo G. Kazanietz**[1,6,*]

[1]Department of Systems Pharmacology and Translational Therapeutics, Perelman School of Medicine, University of Pennsylvania, Philadelphia, PA 19104, USA

[2]Department of Medicine, Einstein Medical Center Philadelphia, Philadelphia, PA 19141, USA

[3]Department of Biological Sciences, University of Toledo, Ohio, OH 43606, USA

[4]Division of Thoracic Surgery, Perelman School of Medicine at the University of Pennsylvania, Philadelphia, PA, USA

[5]Centro de Investigaciones Inmunológicas Básicas y Aplicadas, Universidad Nacional de La Plata, CP1900 La Plata, Argentina

[6]Lead contact

SUMMARY

Despite the undisputable role of the small GTPase Rac1 in the regulation of actin cytoskeleton reorganization, the Rac guanine-nucleotide exchange factors (Rac-GEFs) involved in Rac1-mediated motility and invasion in human lung adenocarcinoma cells remain largely unknown. Here, we identify FARP1, ARHGEF39, and TIAM2 as essential Rac-GEFs responsible for Rac1-mediated lung cancer cell migration upon EGFR and c-Met activation. Noteworthily, these Rac-GEFs operate in a non-redundant manner by controlling distinctive aspects of ruffle dynamics formation. Mechanistic analysis reveals a leading role of the AXL-Gab1-PI3K axis in conferring pro-motility traits downstream of EGFR. Along with the positive association between the overexpression of Rac-GEFs and poor lung adenocarcinoma patient survival, we show that FARP1 and ARHGEF39 are upregulated in EpCam^{+} cells sorted from primary human lung

*Correspondence: rafael.garciamata@utoledo.edu (R.G.-M.), marcelog@upenn.edu (M.G.K.).

AUTHOR CONTRIBUTIONS

Conceptualization, M.C., G.K.-L., M.J.B., N.T.S., E.E., M.C.A., S.M.G., R.G.-M., and M.G.K. Investigation, M.C., G.K.-L., M.J.B., S.Z., N.T.S., and S.M.G. Methodology, M.C., G.K.-L., M.J.B., M.C.A., and S.M.G. Formal analysis, M.C., G.K.-L., M.J.B., M.C.A., R.G.-M., and M.G.K. Writing, M.C., G.K.-L., M.J.B., S.Z., N.T.S., E.E., M.C.A., S.M.G., R.G.-M., and M.G.K. Visualization, M.C., G.K.-L., M.J.B., S.Z., N.T.S., and S.M.G. Resources, N.T.S., E.E., R.G.-M., and M.G.K. Data curation, M.C.A. Funding acquisition, E.E., M.C.A., R.G.-M., and M.G.K. Supervision, M.C., E.E., R.G.-M., and M.G.K. Project administration, M.C., R.G.-M., and M.G.K.

SUPPLEMENTAL INFORMATION

Supplemental information can be found online at https://doi.org/10.1016/j.celrep.2021.109905.

DECLARATION OF INTERESTS

The authors declare no competing interests.

adenocarcinomas. Overall, our study reveals fundamental insights into the complex intricacies underlying Rac-GEF-mediated cancer cell motility signaling, hence underscoring promising targets for metastatic lung cancer therapy.

Graphical Abstract

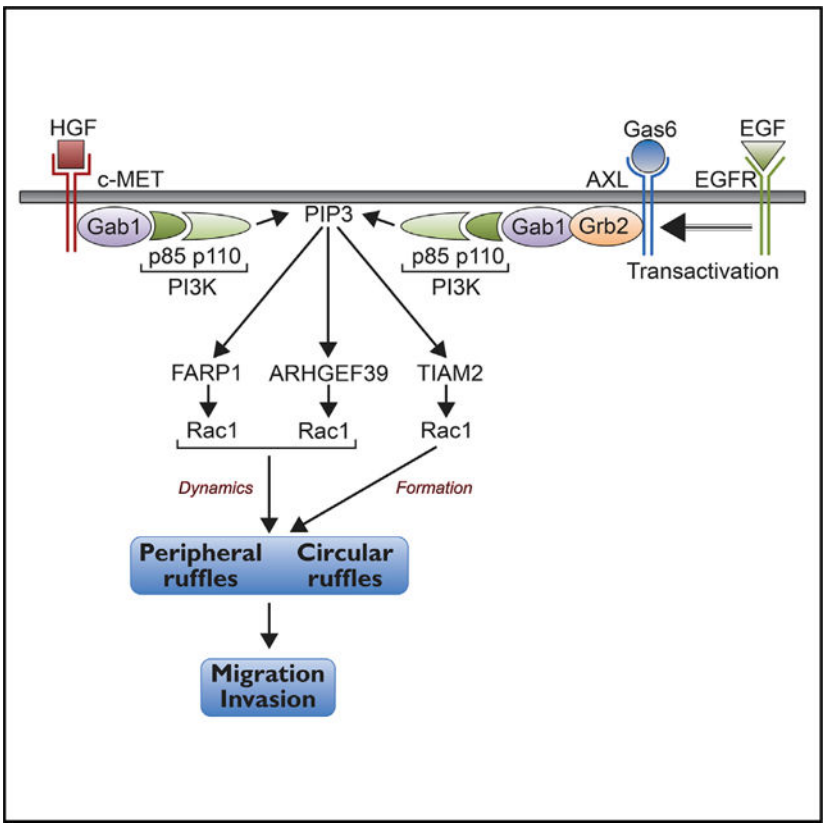

In brief

Cooke et al. identify FARP1, ARHGEF39, and TIAM2 as key drivers of motility signaling in lung adenocarcinoma cells in response to the stimulation of tyrosine kinase receptors (EGFR, c-MET, AXL). These Rac-GEFs operate in a non-redundant manner by controlling distinctive aspects of ruffle dynamics.

INTRODUCTION

Cancer cell motility and invasiveness are stringently regulated events that depend on the dynamic reorganization of the actin cytoskeleton, a process tightly controlled by GTPases of the Rho family. Rac1, a widely expressed Rho guanosine triphosphatase (GTPase), is a major player in the assembly of actin-rich membrane protrusions (i.e., ruffles) implicated in cancer cell migration (Olson and Sahai, 2009; Haga and Ridley 2016; Lawson and Ridley, 2018; Innocenti, 2018). Like most GTPases, Rac1 is a molecular switch that cycles between active GTP-bound and inactive guanosine diphosphate (GDP)-bound states. Growth factors and other extracellular stimuli activate Rac1 via guanine nucleotide exchange factors

(GEFs), whose role is to promote GDP dissociation to allow GTP binding. Active GTP-bound Rac1 subsequently propagates motility signals via downstream effectors such as the p21-activated kinases (PAKs) (Radu et al., 2014; Kazanietz and Caloca, 2017; Marei and Malliri, 2017; Bustelo, 2018). With the exception of a few cases of Rac1 mutations (e.g., $Rac1^{P29S}$ in melanoma), aberrant Rac1 activation in cancer cells involves an excessive upstream input from the deregulated activation of receptor tyrosine kinases (RTKs) and/or their effectors such as phosphatidylinositol 3-kinase (PI3K) (Kazanietz and Caloca, 2017; Bustelo, 2018; Casado-Medrano et al., 2018; Hodge et al., 2020; Cannon et al., 2020).

The Rac-GEF family comprises >40 members, most of them belonging to the Dbl-like class, which has a prototypical DH (Dbl homology) domain responsible for GDP/GTP exchange activity, often in tandem with a PH (pleckstrin homology) domain acting primarily as binding sites for PI3K lipid products (Rossman et al., 2005). Additional domains present in Rac-GEFs likely allow signal diversity and function specificity (Cook et al., 2014; Casado-Medrano et al., 2018). Deregulated Rac-GEF activity in cancer cells, either by overexpression, mutation, or aberrant upstream inputs, has been causally associated with invasive and metastatic phenotypes (Rossman et al., 2005; Cook et al., 2014; Bustelo, 2018; Casado-Medrano et al., 2018; Maldonado and Dharmawardhane, 2018; Cooke et al., 2020). The large repertoire of Rac-GEFs and their diverse cell-type-dependent expression raises the question of which member(s) of the family drive motility signaling in different types of cancer in which deregulated receptor signaling plays a central role.

Lung cancer is the leading cause of cancer-related deaths worldwide. Non-small cell lung cancer (NSCLC) is the most common type of lung cancer, with adenocarcinomas representing the most frequent histological type. Disease is often diagnosed in an advanced stage, with a 5-year relative rate survival <5% (Riihimäki et al., 2014; Gridelli et al., 2015; Lim et al., 2018). Oncogenic alterations in NSCLC include mutations in Kirsten rat sarcoma viral oncogene homolog (KRAS) (~20%–30%) and epidermal growth factor receptor (EGFR) (10%–30%), c-Met and AXL amplifications (1%–5%), and ALK translocations (3%–7%), among others (Gridelli et al., 2015; Kim et al., 2016; Oberndorfer and Müllauer, 2018). In cancer cells, Rac1 is a bona fide effector of RTKs, including EGFR, c-Met, platelet-derived growth factor (PDGFR), and AXL (Yang et al., 2006; Caino et al., 2012; Abu-Thuraia et al., 2015; Li et al., 2018; Hernández et al., 2018), and is also an established effector of mutant KRAS for lung oncogenesis (Kissil et al., 2007). Despite clinical evidence indicating mutual exclusivity for KRAS and EGFR mutations (Suda et al., 2010; Scheffler et al., 2019), a strong dependence on EGFR signaling for KRAS mutant NSCLC growth exists both in cellular models and tumors (Kruspig et al., 2018; Moll et al., 2018; Kharbanda et al., 2020). c-Met and AXL can be also highly expressed and/or hyperactive in KRAS mutant NSCLC tumors and contribute to disease progression (Suzawa et al., 2019; Bahcall et al., 2018; Yang et al., 2019). The intricate RTK-signaling effector networks leading to Rac1-mediated ruffle formation and motility in NSCLC cells remains puzzling, largely due to the scarce information about the expression and functional relevance of Rac-GEFs in this cancer subtype.

Here, we carried out a comprehensive and systematic analysis to ascertain the expression of Rac-GEFs in human lung adenocarcinoma cells and their involvement in Rac1-dependent

motility signaling. This approach led to the unanticipated identification of three Rac-GEFs largely understudied in lung cancer as mediators of ruffle formation in response to EGF and hepatocyte growth factor (HGF), motility, and invasion. A thorough scrutiny of RTK adaptors and effectors revealed key signaling nodes involved in the activation of Rac-GEF/Rac1 in lung adenocarcinoma cells.

RESULTS

Ruffle formation in lung adenocarcinoma cells is PI3K/Rac1 dependent and RhoG independent

Toward the goal of establishing the signaling events leading to the activation of Rac1-mediated responses in lung adenocarcinoma cells, we analyzed the formation of actin-rich ruffles promoted by different growth factors. A prominent induction of ruffle formation, as determined by phalloidin staining, was observed upon stimulation with EGF and HGF in A549 (Figure 1A), H358, and H1299 cells (Figure S1A). Treatment with PDGF caused reduced ruffle forming activity when compared to HGF or EGF (Figure 1A). Standardization of time and concentration dependence is shown in Figure S1B. As a positive control, we used the phorbol ester phorbol 12-myristate 13-acetate (PMA), which caused a strong ruffle response (Caino et al., 2012). To unambiguously establish the Rac1 dependency of this effect, we generated Rac1-deficient A549 cells using CRISPR/Cas9 (Baker et al., 2020). The ruffle formation response by growth factors or PMA was essentially abolished in two different knockout (KO) (Rac1 sgRNA) A549 clones while still present in control (scrambled sgRNA) A549 cells (Figure 1A). Since the Rac-related G protein RhoG has been linked to ruffle formation (Meller et al., 2008; Valdivia et al., 2017; Bagci et al., 2020) and lung adenocarcinoma invasive signaling (Chen et al., 2018), we asked whether it played any role in the growth factor response. However, the experiments shown in Figure 1B revealed that silencing RhoG (>90% depletion) from A549 cells had no effect on the formation of actin-rich structures formed in response to growth factors or PMA. In addition, the ruffle formation activities of EGF, HGF, and PMA were abolished by pre-treatment with the PI3K inhibitor LY294002 as well as by specific inhibitors in each case (gefitinib for EGFR, SU11274 for the HGF receptor c-Met, Gö6983 for protein kinase C [PKC]) (Figure 1C).

Both EGF and HGF promoted the activation of the Rac1 effector PAK in A549 cells. This effect was drastically reduced in Rac1 KO A549 cells (Figure 1D). However, and consistent with the lack of involvement of RhoG in ruffle formation, RhoG-deficient A549 cells retained full PAK activation by the growth factors (Figure 1E). To extend these results to a functional context, cell migration was evaluated using a Boyden chamber assay. As shown in Figure 1F, the migratory capacity of A549 cells was largely impaired in Rac1 KO cells relative to control cells. Conversely, silencing RhoG expression had no effect on A549 cell migration (Figure 1G). These results established that growth factor-mediated formation of actin protrusions and motility signaling requires PI3K and Rac1, but it is independent of RhoG.

Differential utilization of RTK adaptors and effectors in Rac1-mediated ruffle formation

The mechanistic basis of Rac1 signaling activation downstream of RTKs in lung adenocarcinoma cells has been poorly studied. We examined the role of RTK adaptors using a transient RNAi silencing approach. Knocking down the expression of SHC1, Nck1, Grb2, or Gab1, well-established adaptors for EGFR and c-Met (Trusolino et al., 2010; Roskoski, 2014; Reddy et al., 2016) revealed Gab1 as the only common adaptor involved in EGF- and HGF-induced ruffle formation. Silencing Grb2 and SHC1 only affected the EGF response (Figure 2A). The requirement of Gab1 as EGF and HGF effectors was confirmed with three independent small interfering RNA (siRNA) duplexes (Figure S2A).

Tyrosine phosphorylation of the scaffolding Gab1 upon RTK stimulation provides docking sites for effector proteins, including the p85 PI3K subunit and SHP2 (Gu and Neel, 2003). If fact, Gab1^{Y659} phosphorylation, as well as increased phosphorylated levels of the PI3K effector Akt and SHP2, could be readily observed in response to EGF or HGF (Figure 2B). Notably, PAK activation by EGF or HGF was markedly reduced in Gab1 knockdown (KD) cells. Likewise, Akt activation was also dependent on Gab1 (Figure 2C), suggesting that the PI3K dependency for PAK activation involves this adaptor. Despite SHP2 becoming phosphorylated (i.e., activated), SHP2 KD A549 cells retained a full ruffle activation response by either EGF or HGF (Figure 2A), denoting the Gab1-PI3K link as a main axis commonly activated by EGFR and c-Met toward motility signaling.

The requirement of Grb2 for EGF-mediated ruffle formation signaling prompted us to assess its potential involvement in motility signaling. Grb2 not only acts as an adaptor upstream of the mitogenic Raf/MEK/Erk cascade but could also serve as an intermediate RTK adaptor for Gab1 (Kondo et al., 2008). Silencing Grb2 using two different siRNA duplexes led to a significant reduction in EGF-induced activation of PAK and Akt. However, PAK and Akt phosphorylation by HGF was not significantly affected in Grb2 KD cells, corresponding with the lack of involvement of Grb2 in HGF-mediated ruffle formation (Figures 2D and S2B). Moreover, Gab1 phosphorylation by EGF was essentially lost in Grb2 KD cells, whereas its response to HGF was barely affected (only one Grb2 duplex had a small measurable effect) (Figure 2E). These results are consistent with Grb2-Gab1 acting as tandem adaptors for EGFR-motility signaling. Despite this Grb2 requirement, SOS1 RNAi depletion had no impact on ruffle formation by either EGF or HGF (Figure 2A), arguing that these responses are independent from the SOS1/Raf/MEK/ERK cascade.

Studies in breast cancer and glioblastoma models reported transactivation of the RTK AXL, a member of the TAM family receptors, by EGFR and c-Met (Meyer et al., 2013; Li et al., 2018). Given this established partnership, we sought to investigate whether ruffle formation by growth factors in lung adenocarcinoma cells involves AXL. Interestingly, while HGF-mediated ruffle formation was not affected by AXL RNAi silencing, the EGF ruffling response was markedly reduced (Figure 2A). These results indicate differential signaling coupling by EGFR- and c-Met-mediated motility signaling, whereby EGFR signals via AXL transactivation and a Grb2-Gab1-PI3K-dependent pathway.

Identification of FARP1, ARHGEF39, and TIAM2 as mediators of RTK-induced ruffle formation in lung adenocarcinoma cells

There is limited information about the expression and functional relevance of Rac-GEFs in NSCLC. To tackle this issue, we developed a “Rac-GEF” qPCR array to simultaneously determine the expression of 32 Dbl-like Rac-GEFs. This analysis was carried out using mRNA purified from 14 lung adenocarcinoma cell lines with different oncogenic alterations. These experiments revealed ECT2, TRIO, PLEKHG2, VAV2, and FARP1 as the top 5 expressed Rac-GEFs. A similar expression pattern was generally observed in KRAS/NRAS mutant, EGFR mutant, and EML-ALK^{+} cell lines (Figure 3A), arguing that the nature of the oncogenic NSCLC driver may not globally influence Rac-GEF expression.

To determine the involvement of Rac-GEFs in the formation of actin-rich protrusions, we carried out a systematic analysis of growth factor-induced ruffle formation upon RNAi silencing of the top 22 candidates based on the expression screening (top 16 shown in Figure 3B, left panel; additional Rac-GEFs in Figure S3A). Quantitative determination of ruffle formation in response to HGF revealed 3 “hits”: FARP1 (PLEKHC2), ARHGEF39 (C9orf100), and TIAM2 (STEF) (Figure 3B, right panel). Surprisingly, Rac-GEFs widely involved in cancer progression, namely ECT2, TRIO, TIAM1, VAV isoforms, and P-REX isoforms (Sosa et al., 2010; Cook et al., 2014; Bustelo, 2018), were either poorly expressed in lung adenocarcinoma cells (Figure 3A) and/or dispensable for ruffle formation (Figure 3B, right panel). Of note, the requirement for FARP1, ARHGEF39, and TIAM2 was seen in response to multiple growth factors (Figure 3C). These results were validated using three different siRNA duplexes (Figures 3D and S3B). We did not find any significant mutual regulation of Rac-GEF expression by knocking down each one specifically (Figure S3C). A similar Rac-GEF requirement for ruffle formation was observed in additional NSCLC cell lines, albeit with different magnitudes in each case (Figure S3D). The simultaneous silencing of FARP1, ARHGEF39, and TIAM2 (triple KD; Figure 3E) caused strong inhibition both for EGF- and HGF-induced ruffle formation (Figure 3F).

To determine whether the Rac-GEFs localize to ruffles, we used confocal microscopy in A549 cells overexpressing yellow fluorescent protein (YFP)-tagged FARP1, ARHGEF39, or TIAM2 (Figure 4A). Our results revealed that both YFP-fused FARP1 and ARHGEF39 exhibit cytosolic localization in unstimulated cells, and redistribute to the plasma membrane and to ruffles upon stimulation with either EGF or HGF, as determined by phalloidin co-localization (see enlarged insets in Figure 4A and line scans in Figure S4A). Even though ectopically expressed YFP-TIAM2 was sufficient to induce a major ruffling activity response in unstimulated cells and co-localizes with phalloidin, these ruffles redistributed to the cell edge when treated with either EGF or HGF (Figure 4A). While this may suggest a high basal activity for TIAM2 when overexpressed, it also underlines its potential ability to localize in actin-rich ruffle structures and to respond to growth factors, as also observed for FARP1 and ARHGEF39. TIAM2 localization to ruffles in unstimulated cells is lost upon treatment with LY294002, which suggests that it is regulated by PI3K (Figure S4B).

Assessment of Rac1 activation by EGF using a p21-binding domain (PBD) pull-down assay in Rac-GEF KD cells revealed that only FARP1 depletion reduced Rac1-GTP levels significantly (Figure S4C). This result underscores the prominent role of FARP1 in Rac1

activation and motility signaling in lung adenocarcinoma cells. However, a drawback of this assay is that measuring “global” Rac1-GTP cellular levels may underestimate the contribution of distinctive intracellular Rac1 pools regulated by ARHGEF39 or TIAM2. Also, the pull-down assay may not be sensitive enough to detect small changes in Rac1 activity resulting from single Rac-GEF depletion. Due to this limitation, we analyzed the spatial and temporal dynamics of Rac1 activation in live cells using a Rac1 Förster resonance energy transfer (FRET) biosensor (Baker et al., 2020). We generated stable A549 cells expressing low levels of the biosensor and analyzed the effect of EGF stimulation. In parental A549 cells, EGF caused a time-dependent activation of Rac1 at peripheral protrusions in a PI3K-dependent manner (Figure S4D; videos in Data S1). Remarkably, FRET experiments determined that silencing any of the three GEFs abolished EGF-dependent Rac1 activation (Figure 4B; videos in Data S2). Overall, these results support the role of these three GEFs in mediating Rac1 activation downstream of EGFR.

FARP1, ARHGEF39, and TIAM2 are required for lung adenocarcinoma cell migration and invasion

We next examined the migratory capacity of FARP1, ARHGEF39, and TIAM2 KD cells using three different lung adenocarcinoma cellular models (A549, H358, and H1299). Boyden chamber experiments revealed that migration was markedly impaired upon the depletion of each individual Rac-GEF in all three cell lines (Figure 4C). As a control, knocking down TRIO, a Rac-GEF expressed at high levels in these cells (see Figure 3A), had no effect on cell migration, which agrees with its dispensability for ruffle formation (see Figure 3B). We also examined the requirement of these Rac-GEFs for cell invasion using a Boyden chamber assay with Matrigel. Silencing the expression of FARP1, ARHGEF39, or TIAM2 individually led to a marked reduction in the invasive capacity of A549 cells (Figure 4D), again indicating a prominent dependence on these Rac-GEFs.

To further address the involvement of Rac-GEFs in growth factor-mediated motility, we used a quantitative, time-dependent wound assay approach. Both EGF and HGF stimulated A549 cell motility by ~4- to 5-fold relative to basal (serum-starved, unstimulated) conditions, an effect that remained linear for at least 12 h (Figure 5A). Notably, the stimulation of motility by either EGF or HGF was significantly impaired in A549 cells subjected to FARP1, ARHGEF39, or TIAM2 RNAi. A quantitative analysis revealed a 40%–70% reduction in migratory velocity rates upon individual silencing of each Rac-GEF, thus authenticating the relevance of FARP1, ARHGEF39, and TIAM2 as RTK effectors in lung adenocarcinoma cells.

FARP1, ARHGEF39, and TIAM2 differentially regulate ruffle lifetime and size

The lack of compensatory effects upon individual silencing of FARP1, ARHGEF39, and TIAM2 suggests that they should be promoting ruffle formation through non-redundant mechanisms. To determine whether these Rac-GEFs act on different aspects of ruffle dynamics (Figure 5B), we carried out a thorough live imaging analysis in EGF-treated A549 cells expressing the ruffle marker cortactin fused to mCherry. We observed that silencing FARP1 or ARHGEF39, but not TIAM2, significantly decreased ruffle lifetime (Figure 5C) and maximum ruffle area relative to non-target control (NTC) cells (Figure 5D). Analysis of

the assembly rate revealed that it was significantly slower in FARP1 KD cells. The assembly rate also trended lower, although not statistically significant ($p = 0.08$) in ARHGEF39 KD cells, whereas no appreciable changes were observed in TIAM2 KD cells (Figure S5A). None of the three Rac-GEFs appear to play a role in ruffle disassembly (Figure S5B). The stability phase was significantly shorter in both FARP1 and ARHGEF39 KD cells, but not in TIAM2 KD cells (Figure S5C). The shorter ruffle lifetime and size observed in FARP1 and ARHGEF39 KD cells, together with the slower assembly rate and shorter stability, may account for some of the decreased number of ruffles observed at defined time points in fixed cells.

We also analyzed the time of initiation of ruffles after the addition of EGF, which shows a general delay after knocking down either of the three GEFs. While in NTC cells, ~51% of the ruffles emerge within the first 10 min, only 23%, 21%, and 15% of the ruffles form in FARP1, ARHGEF39, and TIAM2 KD cells, respectively, during this time period (Figure 5E). This delay may also contribute to the global reduction in ruffle formation observed in all Rac-GEF KD cells at fixed times.

Differential involvement of FARP1, ARHGEF39, and TIAM2 in the formation of peripheral and circular ruffles

A careful assessment of ruffle dynamics in live cells revealed the formation of two different types of membrane protrusions in response to EGF, namely ruffles associated with the cell edges (“peripheral”) and others having a more circular appearance that originate in the center of the cell, with no apparent contact with the cell edge (“circular”) (Figure 5F; Video S1). In terms of relative abundance, the majority of the ruffles formed in A549 cells were peripheral (percentage peripheral versus percentage circular ruffles: NTC, 80% versus 20%; FARP1 siRNA, 75% versus 25%; ARHGEF39 siRNA, 81% versus 19%; TIAM2 siRNA, 68% versus 32%; not significant versus NTC). These two populations of ruffles appear to display unique properties. Specifically, circular ruffles assembled at significantly faster rates (Figure 5G, NTC), whereas disassembly rate, stability, lifetime, and maximum area were not statistically different between circular and peripheral ruffles (Figures 5H–5K, NTC). The differential dynamics between circular and peripheral ruffles is illustrated in an analysis of all of the variables combined by means of principal-component analysis (PCA) (Figure S5D).

Interestingly, distinct aspects of peripheral versus circular ruffle dynamics were affected, depending on which Rac-GEF has been silenced. First, the assembly rate of circular ruffles was prominently reduced in FARP1 KD cells, with a similar trend observed in ARHGEF39 KD cells (Figure 5G), whereas disassembly rates remained unchanged in all Rac-GEF KD cells (Figure 5H). Second, both FARP1 and ARHGEF39 KD cells had shorter stability phases, albeit only in peripheral ruffles (Figure 5I), probably explaining their reduced lifetime (Figure 5J). Conversely, the effect of the Rac-GEF KD on the lifetime of circular ruffles was less severe, with only ARGHEF39 KD cells showing a statistically significant reduction (Figure 5J). These results also suggest that the overall ruffle lifetime changes in FARP1 and ARHGEF39 KD cells may be mostly driven by the reduction in the lifetime of peripheral ruffles, which are more abundant. Third, FARP1 had a prominent role in the

control of maximum ruffle area. Both circular and peripheral ruffles were smaller in FARP1 KD cells, whereas only the maximum area of peripheral ruffles was reduced in ARHGEF39 KD cells (Figure 5K). It is interesting to note that the decreased assembly rate observed in FARP1 KD circular ruffles did not result in lifetime changes, whereas the opposite was true for peripheral ruffles—in other words, the assembly rate remains unchanged, but the lifetime is reduced, probably a result of the shortened stability phase (Figure 5I). Lastly, despite the impaired ruffle formation in TIAM2 KD cells, the few ruffles that form, either circular or peripheral, displayed properties similar to those of NTC cells. This suggests that TIAM2 has a permissive role rather than directly affecting the dynamics of ruffle formation. A detailed summary of ruffle dynamics data is presented in Table S1.

Characterization of Rac-GEFs as AXL effectors

Given the requirement of the RTK AXL in EGFR-driven ruffle formation in lung adenocarcinoma cells (see Figure 2A), we further explored the relevance of this axis in Rac1 signaling. AXL expression in lung cancer is associated with advanced disease stage and poor clinical outcomes. In addition, AXL activation by its cognate ligand Gas6 has been linked to motile and invasive phenotypes (Ishikawa et al., 2013; Levin et al., 2016; Kanzaki et al., 2017). The requirement of AXL for ruffle formation by EGF but not HGF, as determined with two independent siRNA duplexes (Figure 6A), was recapitulated by using R428, a small inhibitor of catalytic AXL activity (Figure 6B, quantification in Figure S6A). Consistent with this finding, R428 also reduced EGF-induced activation of PAK and Akt (Figure 6C, quantification in Figure S6B). Despite the observed AXL dependency for the EGF response in A549 cells, we noticed that the Gas6 ruffling response was lower than that triggered by EGF. A greater Gas6 response was observed in H1299 cells (Figure S6C), as expected from the higher AXL expression in this cell line compared to A549 cells (Figure S6D). The H1299 cell line was subsequently selected for Gas6-mediated motility studies.

Gas6-induced ruffle formation in H1299 cells was markedly reduced by the PI3K inhibitor LY294002 (Figure 6D, quantification in Figure S6E) as well as by Gab1 or Grb2 silencing (Figure 6E). As expected, the effect of Gas6 in H1299 cells was abrogated by AXL RNAi or R428 treatment (Figure S6F). Gas6, like EGF, promotes strong phosphorylation of Akt, PAK, and Gab1 in H1299 cells (Figure 6F). The signaling effects of Gas6 were greater than those of HGF and PDGF in these cells (Figure S6G). We observed that activation of PAK and Akt by Gas6 in H1299 cells was impaired by PI3K inhibition with LY294002 (Figure 6G, quantification in Figure S6H). Likewise, Gab1 RNAi depletion impaired PAK and Akt activation by Gas6 and EGF in H1299 cells (Figure S6I), as shown above in A549 cells. Analysis of Gas6-induced ruffle formation in Rac-GEF KD H1299 cells showed a clear dependence on FARP1 and TIAM2. ARHGEF39 KD H1299 cells showed a trend toward a lower Gas6-mediated ruffle response, although it did not reach statistical significance ($p = 0.08$; Figure 6H).

Gas6 enhanced motility by ~2-fold relative to basal (serum-starved) in H1299 cells. FARP1 RNAi silencing essentially abolished Gas6-stimulated motility without affecting basal motility (Figure 6I). Silencing FARP1 from H1299 cells also led to a marked inhibition of PAK activation by Gas6 (Figure 6J). Remarkably, treatment of H1299 cells expressing

YFP-FARP1 with Gas6 caused a pronounced redistribution of this Rac-GEF to membrane ruffles, which showed co-localization with the ruffle marker cortactin (Figure 6I). FARP1 translocation to ruffles could not be detected in H1299 cells treated with the PI3K inhibitor LY294002 or subjected to Gab1 RNAi silencing (Figure 6K; Videos S2 and S3).

Rac-GEF expression in primary human lung adenocarcinoma

Analysis of the human lung adenocarcinoma GEO: GSE31210 dataset revealed that 13 of the 32 Dbl-family Rac-GEFs display statistically significant upregulation in tumors versus normal tissue (Figures 7A and 7B, full list in Table S2). Noteworthily, FARP1, ARHGEF39, and TIAM2 were among the Rac-GEFs upregulated in lung tumors, as visualized in the corresponding box-plots displayed in Figure 7C. This bioinformatics analysis also identified ARHGEF39 as the top negative predictor for poor overall survival (OS) and disease-free survival (DFS) among all 32 Dbl-like Rac-GEFs (Figures 7B and S7). Despite their involvement in motility/invasion signaling, neither FARP1 nor TIAM2 expression have any prognostic correlations.

Finally, we determined the expression of FARP1, ARHGEF39, and TIAM2 in tumor cells isolated from fresh surgically resected human lung adenocarcinomas. Using a combined approach that involves anti-EpCam$^+$ microbeads and fluorescence-activated cell sorting (FACS), EpCam$^+$ cells were isolated with >95% purity from the tumors as well as from the corresponding normal adjacent tissue, and cDNA prepared from the samples. qPCR analysis revealed a marked upregulation of FARP1 and ARHGEF39 mRNA levels in a significant proportion of EpCam$^+$ tumor samples relative to EpCam$^+$ cells from normal adjacent tissue (Figure 7D). Cycle threshold (Ct) values for TIAM2 were generally >34 cycles, and thus results were considered unreliable. This probably reflects its lower overall expression compared to the other Rac-GEFs. As a control, the Rac-GEF PREX1 did not display upregulation in tumor EpCam$^+$ cells, as also predicted from the database analysis (see Table S2), thus underlining the upregulation of selected Rac-GEFs in primary human lung adenocarcinoma.

DISCUSSION

Our study identified the Rac-GEFs responsible for the formation of actin-rich ruffles by RTK stimulation in human lung adenocarcinoma. Only three Rac-GEFs displayed an essential requirement for growth factor promotion of ruffle formation. FARP1, ARHGEF39, or TIAM2 silencing not only altered the reorganization of the actin cytoskeleton into protrusive structures but also impaired lung adenocarcinoma cell motility and invasiveness. To our surprise, well-studied pro-motility/invasive Rac-GEFs turned out to be dispensable. This may be explained by their relatively low expression in lung adenocarcinoma cells compared to other cancer cell types (e.g., P-REX1 and VAV3, which are highly expressed in breast cancer cells) (Sosa et al., 2010; Citterio et al., 2012) and/or the lack of compensatory mechanisms by other GEFs upon individual Rac-GEF silencing. The latter would be expected based on the differential regulation and localization of structurally related Rac-GEFs such as TIAM1 and TIAM2 (Shepherd et al., 2011; Maltas et al., 2020). Interestingly, FARP1, ARHGEF39, and TIAM2 Rac-GEFs act as downstream effectors

of RTKs such as EGFR and c-Met. We speculate that other highly expressed Rac-GEFs in lung adenocarcinoma cells may contribute to disease progression through functions unrelated to actin cytoskeletal reorganization. An interesting example is ECT2, the highest expressed Rac-GEF in lung adenocarcinoma cells, which plays fundamental roles in lung tumorigenesis by promoting ribosomal RNA (rRNA) synthesis at the nucleolus (Justilien et al., 2017).

Whereas early studies reported ARHGEF39 and TIAM2 to be involved in lung cancer cell migration (Zhao et al., 2013; Zhou et al., 2018), FARP1 had not been previously associated with lung cancer. FARP1 has been mostly involved in neuronal development, particularly in the control of synaptogenesis, dendritic filopodial dynamics, and branching (Cheadle and Biederer, 2012, 2014), and more recently in the regulation of endothelial integrity (Amado-Azevedo et al., 2017). A recent report showed FARP1 to boost Cdc42 activity and filopodia formation in advanced gastric cancer (Hirano et al., 2020), an observation that we were unable to observe in lung adenocarcinoma cells (unpublished data). The consistent impairment in membrane ruffling activity and Rac1/PAK activation in FARP1-depleted lung adenocarcinoma cells upon the stimulation of multiple RTKs strongly advocates for its role as a positive regulator of a Rac1 centered signaling unit, as suggested in neuronal models (Cheadle and Biederer, 2012).

Another important finding in the present study is the identification of Dbl-like Rac-GEFs as effectors for AXL, an RTK largely associated with metastatic disease, poor clinical outcomes, and targeted therapy resistance in lung adenocarcinoma patients (Ishikawa et al., 2013; Levin et al., 2016; Kanzaki et al., 2017). We found that the AXL natural ligand Gas6 induces a prominent relocalization of FARP1 to ruffle protrusions. The involvement of AXL in EGFR-driven ruffle formation in lung adenocarcinoma cells also attests to its utmost relevance in Rac-GEF/Rac1-mediated motility signaling via transactivation mechanisms. In this context, our results established PI3K as a common link between RTKs for Rac-GEF activation, consistent with the presence of DH-PH domains in FARP1, ARHGEF39, and TIAM2. It is well known that PH domains in Rac-GEFs play crucial roles in binding PI3K phosphoinositide products, or in some cases, in binding to activating proteins as well as in autoinhibition (Rossman et al., 2005; Cook et al., 2014). We also found a striking dependence on the adaptor Gab1 for ruffle formation for all RTKs examined, including AXL. Gab1, which engages the p85 PI3K subunit and subsequent activation of the PI3K/Akt pathway upon growth factor stimulation, can mediate motility signaling upstream of Rac1 (Kallin et al., 2004; Watanabe et al., 2006; Abella et al., 2010). Our results show a differential RTK requirement for other adaptors, such as Grb2 for EGFR but not for c-Met, which fits with the reported Gab1 recruitment via Grb2-dependent or Grb2-independent mechanisms (Lock et al., 2000; Sampaio et al., 2008). In summary, Gab1/PI3K represents the central node for Rac-GEF activation in lung adenocarcinoma cells (Figure 7E). However, at this point we cannot rule out unique mechanisms leading to Rac1 activation driven by other Rac-GEF hubs.

Irrespective of the common activation mechanisms, the considerable divergence in their domain architecture between FARP1, ARHGEF39, and TIAM2 strongly argues for unique modes of regulation in each case. For instance, membrane association studies with FARP1

revealed a stringent requirement for the N-terminal FERM domain via phospholipid interactions. The FARP1 FERM domain also interacts directly with cytoplasmic tails of membrane receptors and other proteins (Cheadle and Biederer, 2012, 2014; Kuo et al., 2018), a scenario that has yet to be evaluated in the context of RTK signaling. Conceivably, similar mechanisms could also apply to the multidomain Rac-GEF TIAM2. Notably, we found that the ectopic expression of TIAM2 was sufficient to constitutively form ruffles at sites where this GEF localizes. It is worth noting that remarkable work from Malliri and coworkers (Woroniuk et al., 2018; Maltas et al., 2020) reported endogenous TIAM2 to localize in the outer nuclear membrane to control nuclear re-orientation required for optimal cell migration, which can be observed in our experiments, although the prominent ruffle localization often masks the nuclear signal. While a potential mislocalization of ectopically expressed TIAM2 in our studies cannot be ruled out, we can confidently conclude that this Rac-GEF possesses the structural requirements for localization in membrane ruffles, possibly involving domains engaged in local lipid and/or protein interactions. ARHGEF39, the smallest Dbl-like Rac-GEF, lacks any obvious domain(s) other than a DH-PH tandem domain and also translocates from the cytoplasm to membrane ruffles in response to growth factors. This is suggestive of autoinhibition relief upon RTK stimulation, conceivably involving post-translational modifications. PhosphoSitePlus and phospho-proteomics datasets predict N-terminal phosphorylated sites in ARHGEF39, consistent with established models of GEF autoinhibition relief and relocalization (Rossman et al., 2005; Yohe et al., 2008; Yu et al., 2010; Chow et al., 2013).

A hint for the non-compensatory functional requirement of FARP1, ARHGEF39, and TIAM2 is their differential involvement in the control of ruffle dynamics. Our detailed kinetic analysis of ruffle assembly, disassembly, and stability using live imaging provided a comprehensive portrait that cannot otherwise be obtained at fixed times of stimulation. Our findings suggest that Rac-GEFs may operate at different levels, with FARP1 and ARHGEF39 playing a direct role in the control of ruffle dynamics, and TIAM2 regulating signaling events that may be more binary in nature (Figure 7E). The reduced number of ruffles that still form in TIAM2-depleted cells are indistinguishable from those in control cells and likely represent protrusions formed in cells refractory to TIAM2 RNAi depletion. The identification of two clearly distinguishable types of ruffles with unique properties supports the exciting possibility that they control different biological processes. Based on established dogmas, peripheral ruffles may be vital for cell migration, whereas circular ruffles may have roles in macropinocytosis. The observed selective involvement of discrete Rac-GEFs in the regulation of circular versus peripheral ruffle dynamics suggests that different Rac-GEF/Rac1 complexes may control discrete Rac1-mediated responses. Beyond the scope of these studies, it would be interesting to examine the effects of targeted Rac-GEF inhibition on specific cellular events regulated by Rac1 as well as to mechanistically explore the contribution of different Rac1 subcellular pools to these responses. Recent systems analysis of GEF and GAP regulatory proteins revealed spatially organized Rac1 signaling consistent with function specificity (Müller et al., 2020; Bagci et al., 2020). As suggested, GEFs are mainly autoinhibited to allow local regulation, and form complexes to coordinately regulate functional networks (Müller et al., 2020). In this context, another level of complexity may involve the regulation of specific Rac-GEFs by different receptor classes

(e.g., tyrosine kinases versus G protein-coupled receptors [GPCRs]) by promoting unique signaling associations and interactomes.

In summary, our study identified the essential Rac-GEFs responsible for ruffle formation and motility signaling by RTK stimulation in lung adenocarcinoma cells, acting in a non-redundant manner. The large number of Rac-GEFs expressed in cancer cells epitomizes the requirement of coordinated signals to drive essential processes in tumorigenesis and metastasis. In this regard, the upregulation of selected Rac-GEFs and their associations with poor clinical outcome in lung adenocarcinoma highlights their likely relevance in disease progression. Our systematic approach could be straightforwardly applied to different cancer types to identify disease-specific motility/invasive effectors and fuel the rational design of antineoplastic agents targeted to block Rac-GEF interactions with Rac1 and/or other partners.

STAR★METHODS

RESOURCE AVAILABILITY

Lead contact—Further information and requests for resources and reagents should be directed to and will be fulfilled by Dr. Marcelo G. Kazanietz (marcelog@pennmedicine.upenn.edu).

Materials availability—This study did not generate new unique reagents.

Data and code availability

- This paper analyzes existing, publicly available data. These accession numbers for the datasets are listed in the Key resources table.
- This paper does not report original code.
- Any additional information required to reanalyze the data reported in this paper is available from the lead contact upon request.

EXPERIMENTAL MODELS AND SUBJECT DETAILS

Cell lines—Cell lines are described in the Key resources table. Cells were cultured in RPMI medium supplemented with 10% FBS, 2 mM glutamine, 100 U/ml penicillin and 100 μg/ml streptomycin, at 37°C in a humidified 5% CO_2 atmosphere. PMA was purchased from LC Laboratories (Woburn, MA). 4′,6-Diamidino-2-phenylindole (DAPI) was obtained from Sigma.

Human specimens—EpCam+ cells were sorted from lung adenocarcinomas from patients (male and female, age range: 53–71) with stage I–II lung cancer, who were scheduled for surgical resection. Patients consented to the harvest of a portion of their tumor and blood for research purposes. All patients signed an informed consent document that had been approved by the University of Pennsylvania Institutional Review Board (protocol # 805800). All patients selected for entry into the study met the following criteria: (a)

histologically confirmed adenocarcinoma, (b) no prior chemotherapy or radiation therapy within 2 years, and (c) no other malignancy.

METHOD DETAILS

Western blot assay—Western blots were done essentially as previously described (Cooke et al., 2019). Briefly, cells were harvested in lysis buffer containing 50 mM Tris-HCl, pH 6.8, 10% glycerol, and 2% β-mercaptoethanol. Cell lysates were subjected to SDS-polyacrylamide gel electrophoresis and transferred to polyvinylidene difluoride membranes (Millipore Corporation, Billerica, MA). After blocking with 5% milk or 5% BSA in Tris-buffered saline/0.1% Tween for 1 h, membranes were incubated overnight with primary antibodies. Membranes were then incubated for 1 h with either anti-mouse (1:1,000 dilution) or anti-rabbit (1:3,000 dilution) secondary antibodies conjugated to horseradish peroxidase (Bio-Rad Laboratories, Hercules, CA). Bands were visualized and subjected to densitometric analysis using an Odyssey Fc system (LI-COR Biotechnology, Lincoln, NE).

Rac-GEF Q-PCR array and Q-PCR assays—Total RNA from cultured cells was extracted using the RNeasy kit as directed by the manufacturer (QIAGEN, Valencia, CA). One μg of the mRNA template was added to the reverse-transcription master mix (Taq-Man Reverse Transcription kit, QIAGEN). The cDNA samples were then diluted with 90 μL of RNase-free water and stored at −20°C. To quantify the expression Rac-GEFs we used a custom-made Q-PCR array (ThermoFisher Scientific) that encompassed 32 Dbl Rac-GEFs. The array included UBC and B2M housekeeping genes for normalization.

Q-PCR amplifications were performed using an ABI PRISM 7300 Detection System in a total volume of 20 μL containing Taqman Universal PCR Master Mix (ThermoFisher Scientific). PCR product formation was continuously monitored using the Sequence Detection System software version 1.7 (Applied Biosystems). Results were expressed as ΔCt, which was calculated as the difference in Ct values between the Rac-GEF of interest and the average of housekeeping genes.

RNA interference—For silencing the expression of individual targets, we used previously validated ON-TARGET Plus siRNA sequences from Dharmacon (Lafayette, CO). siRNA duplexes were transfected using Lipofectamine RNAi Max (Invitrogen, Carlsbad, CA). Experiments were carried out 48 h after transfection. siRNA duplexes were used at a concentration of 25 nM, except for triple knockdown experiments (10 nM for each Rac-GEF duplex, 30 nM for NTC).

Phalloidin staining—Assessment of morphological cytoskeletal changes was done as described before (Caino et al., 2012; (Cooke et al., 2018)). Briefly, cells growing on glass cover slides at low confluency were serum starved for 24 h and stimulated with the corresponding growth factor at the indicated concentrations. Following fixation with 4% formaldehyde, F-actin was stained with phalloidin-rhodamine and nuclei were counterstained with DAPI. Slides were visualized by fluorescence microscopy and 5 random fields were scored for the number of ruffles. Ruffle area was measured by thresholding for signal intensity using ImageJ/Fiji software (Cooke et al., 2018).

Migration and invasion assays—For assessment of migration, we used a Boyden chamber assay, as described (Caino et al., 2012). Briefly, lung adenocarcinoma cells were trypsinized, suspended in 0.1% BSA/RPMI, and seeded (2.5×10^4 cells/well) in the upper compartment of a Boyden chamber (NeuroProbe). A 12-μm-pore polycarbonate membrane was used to separate the upper and lower compartments. In the lower chamber, RPMI medium containing 10% FBS was used. After an incubation period of 16 h at 37°C, membranes were recovered and cells on the upper side of the membrane (non-migrating) were wiped off the surface. Cells on the lower side of the membrane (migrating) were fixed and stained with the Hema 3 Staining kit (Thermo Scientific). Densitometric analysis of stained membrane was done, and results were expressed as arbitrary units (A.U.). For validation, migrating cells in each well were counted in five random fields by contrast microscopy using an Eclipse E200 Nikon microscopy (4X magnification) and the ImageJ/Fiji software. Each condition was assessed at least by triplicate. Every experiment was performed independently three times. For invasion assays, migration was measured using Matrigel-coated polycarbonate membranes, as previously described (Caino et al., 2012; Garg et al., 2017).

For wound assays, confluent cultures of lung adenocarcinoma cells were serum starved for 24 h, and a wound was generated using a sterile p10 tip. Cells were stimulated with EGF, HGF, PDGF or Gas6 and micrographs were taken every 2 h for 12 h using an Eclipse E200 Nikon microscopy (40X magnification). The width of wounds was measured using ImageJ/Fiji software. Migration velocity was determined from the slope of the time-course. At least three independent experiments were performed for each condition.

Rac-GTP pull-down assays—Determination of Rac-GTP levels was carried out essentially as previously described (Caino et al., 2012; Baker et al., 2020). Briefly, cells were transfected with the indicated siRNA duplexes, and 48 h later serum starved for 16 h and treated with EGF (100 ng/ml, 1 min). Cells were lysed in the presence of a recombinant Pak1-binding domain tagged to GST, and lysates were clarified and then incubated for 45 min in the presence of reduced glutathione-Sepharose beads. Beads were washed twice with lysis buffer and run on SDS-PAGE. Rac1 was then assessed by western blot using an anti-Rac1 antibody.

Immunofluorescence studies—YFP-tagged FARP1, TIAM2 or ARHGEF39 (kind gifts of Dr. Oliver Rocks, MDC, Germany) (Müller et al., 2020) were transfected into lung adenocarcinoma cells using TransIT 2020 (Mirus). Following overnight incubation, cells were plated on glass coverslips in complete medium and incubated for 8 h before starving overnight with serum-free medium. The following morning, cells were treated with the indicated growth factors and processed for immunofluorescence. For immunofluorescence, cells were fixed for 10 min with 3.7% paraformaldehyde and quenched with 10 mM ammonium chloride. Cells were then permeabilized with 0.1% Triton X-100 in PBS. The coverslips were then washed with PBS and blocked with PBS/2.5% goat serum/0.2% Tween 20 for 5 min, followed by 5 min of blocking with PBS/0.4% fish skin gelatin/0.2% Tween 20. Cells then were incubated with the primary anti-cortactin antibody for 1 h at room temperature. Coverslips were washed with PBS/0.2% Tween 20 and incubated a secondary

antibody (goat anti-Rabbit IgG (H+L) Cross-Adsorbed Secondary Antibody, Alexa Fluor 594, Invitrogen) for 45 min, washed as described, and mounted on glass slides in Mowiol mounting solution. Images were acquired on an Olympus IX81 inverted microscope using a PlanApo N 60 × 1.42 NA oil objective lens and an Orca Flash 4.0 sCMOS camera (Hamamatsu, Japan), or with a Leica Stellaris 5 laser scanning confocal using a HC PL APO 63x/1.40 OIL CS2 objective. Image processing and quantitative analysis was performed using Fiji.

Live imaging, analysis of ruffle dynamics and principal component analysis (PCA)—Cells were infected with an mCherry-Cortactin-encoding adenovirus (Goicoechea et al., 2017) to visualize membrane ruffles, serum starved, and treated with either EGF (100 ng/ml) or Gas6 (500 ng/ml) at frame 5 of each time-lapse. Ruffle dynamics were imaged using a Nikon Eclipse Ti2 microscope equipped with a Tokai Hit STX stage top incubator, 60x NA1.49 oil immersion objective, Hamamatsu ORCA-Flash 4.0 camera, Lumencor SPECTERA X solid-state light source, and NIS-Elements software. Cells were imaged from 30 randomly selected fields every 30 s for 30 min with 2×2 binning, 3% light intensity and 500 ms exposure. Prior to imaging, cells were treated with 1:100 Oxyfluor reagent (Oxyrase Inc.) and 10 mM dl-lactate (Sigma-Aldrich) to reduce oxygen free radicals and minimize photodamage.

Quantification of ruffle dynamics was done using ImageJ by manually measuring the area of each ruffle over time after treatment. The increase/decrease in area over time was used to calculate ruffle assembly and disassembly rates, as well as stability.

The principal component analysis (PCA) for ruffle dynamics was performed in Rstudio version 1.4.1106 using the prcomp function from the stats package. Ruffles with missing values were discarded. The predict function from the stats package was used to acquire the principal component values for each of the ruffles. The first two principal components were plotted against each other using ggplot2, with ellipses representing 95% confidence intervals.

FRET acquisition and processing—Rac1 activation status was measured using a previously characterized dimerization-optimized reporter for activation (DORA) single-chain Rac1 biosensor (generous gift from Yi Wu, UConn Health, Farmington, CT) (Timmerman et al., 2015). Experiments were carried out as previously described (Baker et al., 2020). Briefly, serum starved A549 cells stably expressing the Rac1 biosensor at low levels, were treated with 100 ng/ml EGF to induce ruffle formation. We used 1:100 Oxyfluor reagent (Oxyrase Inc.) and 10 mM DL-lactate (Sigma-Aldrich) to reduce oxygen free radicals. Cells were imaged every 15 s with 2 × 2 binning and 16-bit depth, using a Nikon Eclipse Ti2 microscope equipped with a Tokai Hit STX stage top incubator, 60x NA1.49 oil immersion objective, Hamamatsu ORCA-Flash 4.0 camera, Lumencor SPECTRA X solid-state light source, and NIS-Elements software. The microscope is equipped with a dichroic splitter to facilitate simultaneous acquisition of Cerulean3 and Venus emissions. Raw images were processed in batch using a custom designed macro in ImageJ, which included corrections to account for background and bleaching, and a median filter with a

2-pixel radius was applied to reduce noise. The FRET ratio was calculated, and a custom LUT was applied to allow for the visualization of Rac1 activation.

Determination of Rac-GEF expression in EpCam+ human lung adenocarcinoma cells—Surgically resected fresh lung tumors and adjacent lung tissue were processed within 20 min of removal from the patient using an optimized disaggregation method (Quatromoni et al., 2015). Briefly, under sterile conditions, all areas of tissue necrosis were trimmed away. The tumor and adjacent uninvolved lung tissue were sliced into 1–2 mm^3 pieces with micro-dissecting scissors equipped with tungsten carbide insert blades (Biomedical Research Instruments, Inc.). For enzymatic digestion, the pieces were incubated in a shaker for 45 min at 37°C in serum-free L-15 Leibovitz media (HyClone) containing enzymes at low concentrations. The enzymatic cocktail for tumor digestion consisted of serum-free Hyclone Leibovitz L-15 media supplemented with 1% penicillin-streptomycin, collagenase type I and IV (170 mg/l = 45–60 U/ml), collagenase type II (56 mg/l = 15–20 U/ml), DNase-I (25 mg/l), and elastase (25 mg/l) (all from Worthington Biochemical). After 45 min, any visible tumor pieces were vigorously pipetted against the side of a 50 mL tube to enhance disaggregation and then further incubated for 30–50 min under the same conditions. Larger pieces of tumor tissue were permitted to settle to the bottom of the tube and the supernatant was passed through a 70 μM nylon cell strainer (BD Falcon). The remaining pieces in the tube underwent further pipetting before being passed through the same cell strainer. Typically, less than 5% of the tissue (consisting of mostly non-cellular connective tissue) remained on the cell strainer. After filtration the red blood cells were lysed using 1x Red Blood Cell (RBC) lysis buffer (Santa Cruz). The remaining cells were washed twice in RPMI supplemented with 2% FBS and re-suspended in the cell culture media. Cell viability, as determined by trypan blue exclusion or Fixable Viability Dye eFluor 450 staining, was typically > 90%. If the viability of cells was less than 80%, dead cells were eliminated using a “dead cell removal kit” (Miltenyi Biotec Inc.).

Live $EpCam^+$ cells were isolated from single cell suspensions by flow cytometric cell sorting-based on the common phenotype of epithelial cells $CD45^-EpCam^+$. Single cell suspension obtained from digested tumor and distant tissue was stained with EPCAM-FITC (Biolegend, clone 9C4) and CD45-BV785 (Biolegend, clone 2D1). Sterile cell sorting was performed on the FACSAria Fusion cell sorter (BD Biosciences). The isolated $EpCam^+$ population were greater than 99% pure. At least 10,000 pure $EpCam^+$ cells were isolated and used for RNA isolation.

Rac-GEF expression levels in EpCam+ cells isolated from human lung tumors was determined by Q-PCR.

***In silico* analysis of Rac-GEF expression profiles in lung adenocarcinomas —**To further explore the relevance of Dbl-like Rac-GEFs genes in lung adenocarcinoma samples, we evaluated their expression profiles in normal and primary tumors derived from an Affymetrix HG-U133 Plus2 based studies composed of early-stage lung adenocarcinoma cases with follow-up data (GSE31210). Pre-processed mRNA expression levels (log2 transformed), clinicopathological, and survival data (OS and DFS) were retrieved from the CancerTools resource (http://genomics.cicbiogune.es/CANCERTOOL/). Up-modulation of

Rac-GEF expression levels between normal (n = 20) and primary tumors (n = 226) was determined using one-tailed t test ($p < 0.05$).

For survival analysis, primary lung adenocarcinomas were divided into two groups (low and high Rac-GEF expression) according to their median expression levels. Survival curves (OS and DFS) were estimated using the Kaplan-Meier method and compared using the log-rank test. Univariate, survival analysis, and data visualization were performed with the R software.

QUANTIFICATION AND STATISTICAL ANALYSIS

Independent experiments were performed at least three times. Statistical significance was determined by Student's t test or ANOVA using GraphPad Prism 8.0. For ruffle dynamics, each dataset was tested for normality using the D'Agostino test. Statistical significance was then determined using either a t test (two-tailed, unpaired), with data that passed the normality test, or a Mann-Whitney U test. For *in silico* analysis of Rac-GEF expression in human lung adenocarcinomas, upregulated expression in tumors was analyzed using a one-tailed t test. Survival curves were estimated using the Kaplan-Meier method and compared using the log-rank test. In all cases, a value of $p < 0.05$ was considered statistically significant.

Supplementary Material

Refer to Web version on PubMed Central for supplementary material.

ACKNOWLEDGMENTS

This work was supported by grants R01-ES026023 (to M.G.K.), R03-CA234693 and R01-GM136826-01 (to R.G-M.) and R01-CA187392 (to E.E.) from the NIH, and PICT-2018-01403 from the Argentine National Agency of Scientific and Technological Promotion (to M.C.A.). M.G.K. also acknowledges support by grant P30 ES013508 from the NIEHS of the NIH. N.T.S. is supported by grant T32 CA009140 from the NIH.

REFERENCES

Abella JV, Vaillancourt R, Frigault MM, Ponzo MG, Zuo D, Sangwan V, Larose L, and Park M (2010). The Gab1 scaffold regulates RTK-dependent dorsal ruffle formation through the adaptor Nck. J. Cell Sci 123, 1306–1319. [PubMed: 20332103]

Abu-Thuraia A, Gauthier R, Chidiac R, Fukui Y, Screaton RA, Gratton JP, and Côté JF (2015). Axl phosphorylates Elmo scaffold proteins to promote Rac activation and cell invasion. Mol. Cell. Biol 35, 76–87. [PubMed: 25332238]

Amado-Azevedo J, Reinhard NR, van Bezu J, de Menezes RX, van Beusechem VW, van Nieuw Amerongen GP, van Hinsbergh VWM, and Hordijk PL (2017). A CDC42-centered signaling unit is a dominant positive regulator of endothelial integrity. Sci. Rep 7, 10132. [PubMed: 28860633]

Bagci H, Sriskandarajah N, Robert A, Boulais J, Elkholi IE, Tran V, Lin ZY, Thibault MP, Dubé N, Faubert D, et al. (2020). Mapping the proximity interaction network of the Rho-family GTPases reveals signalling pathways and regulatory mechanisms. Nat. Cell Biol 22, 120–134. [PubMed: 31871319]

Bahcall M, Awad MM, Sholl LM, Wilson FH, Xu M, Wang S, Palakurthi S, Choi J, Ivanova EV, Leonardi GC, et al. (2018). Amplification of wild-type KRAS imparts resistance to crizotinib in MET exon 14 mutant non-small cell lung cancer. Clin. Cancer Res 24, 5963–5976. [PubMed: 30072474]

Baker MJ, Cooke M, Kreider-Letterman G, Garcia-Mata R, Janmey PA, and Kazanietz MG (2020). Evaluation of active Rac1 levels in cancer cells: a case of misleading conclusions from immunofluorescence analysis. J. Biol. Chem 295, 13698–13710. [PubMed: 32817335]

Bustelo XR (2018). RHO GTPases in cancer: known facts, open questions, and therapeutic challenges. Biochem. Soc. Trans 46, 741–760. [PubMed: 29871878]

Caino MC, Lopez-Haber C, Kissil JL, and Kazanietz MG (2012). Non-small cell lung carcinoma cell motility, rac activation and metastatic dissemination are mediated by protein kinase C epsilon. PLoS ONE 7, e31714. [PubMed: 22384062]

Cannon AC, Uribe-Alvarez C, and Chernoff J (2020). RAC1 as a therapeutic target in malignant melanoma. Trends Cancer 6, 478–488. [PubMed: 32460002]

Casado-Medrano V, Baker MJ, Lopez-Haber C, Cooke M, Wang S, Caloca MJ, and Kazanietz MG (2018). The role of Rac in tumor susceptibility and disease progression: from biochemistry to the clinic. Biochem. Soc. Trans 46, 1003–1012. [PubMed: 30065108]

Cheadle L, and Biederer T (2012). The novel synaptogenic protein Farp1 links postsynaptic cytoskeletal dynamics and transsynaptic organization. J. Cell Biol 199, 985–1001. [PubMed: 23209303]

Cheadle L, and Biederer T (2014). Activity-dependent regulation of dendritic complexity by semaphorin 3A through Farp1. J. Neurosci 34, 7999–8009. [PubMed: 24899721]

Chen Q, Lu X, Liu QX, Zhou D, Qiu Y, Dai JG, and Zheng H (2018). SGEF is a potential prognostic and therapeutic target for lung adenocarcinoma. World J. Surg. Oncol 16, 32. [PubMed: 29454349]

Chow CR, Suzuki N, Kawamura T, Hamakubo T, and Kozasa T (2013). Modification of p115RhoGEF Ser(330) regulates its RhoGEF activity. Cell. Signal 25, 2085–2092. [PubMed: 23816534]

Citterio C, Menacho-Márquez M, García-Escudero R, Larive RM, Barreiro O, Sánchez-Madrid F, Paramio JM, and Bustelo XR (2012). The rho exchange factors vav2 and vav3 control a lung metastasis-specific transcriptional program in breast cancer cells. Sci. Signal 5, ra71. [PubMed: 23033540]

Cook DR, Rossman KL, and Der CJ (2014). Rho guanine nucleotide exchange factors: regulators of Rho GTPase activity in development and disease. Oncogene 33, 4021–4035. [PubMed: 24037532]

Cooke M, Casado-Medrano V, Ann J, Lee J, Blumberg PM, Abba MC, and Kazanietz MG (2019). Differential regulation of gene expression in lung cancer cells by diacyglycerol-lactones and a phorbol ester via selective activation of protein kinase C isozymes. Sci. Rep 9, 6041. [PubMed: 30988374]

Cooke M, Baker MJ, and Kazanietz MG (2020). Rac-GEF/Rac signaling and metastatic dissemination in lung cancer. Front. Cell Dev. Biol 8, 118. [PubMed: 32158759]

Cooke M, Zhou X, Casado-Medrano V, Lopez-Haber C, Baker MJ, Garg R, Ann J, Lee J, Blumberg PM, and Kazanietz MG (2018). Characterization of AJH-836, a diacylglycerol-lactone with selectivity for novel PKC isozymes. J. Biol. Chem 293, 8330–8341. [PubMed: 29636415]

Garg R, Blando JM, Perez CJ, Abba MC, Benavides F, and Kazanietz MG (2017). Protein kinase C epsilon cooperates with PTEN loss for prostate tumorigenesis through the CXCL13-CXCR5 pathway. Cell Rep. 19, 375–388. [PubMed: 28402859]

Goicoechea SM, Zinn A, Awadia SS, Snyder K, and Garcia-Mata R (2017). A RhoG-mediated signaling pathway that modulates invadopodia dynamics in breast cancer cells. J. Cell Sci 130, 1064–1077. [PubMed: 28202690]

Gridelli C, Rossi A, Carbone DP, Guarize J, Karachaliou N, Mok T, Petrella F, Spaggiari L, and Rosell R (2015). Non-small-cell lung cancer. Nat. Rev. Dis. Primers 1, 15009. [PubMed: 27188576]

Gu H, and Neel BG (2003). The “Gab” in signal transduction. Trends Cell Biol. 13, 122–130. [PubMed: 12628344]

Haga RB, and Ridley AJ (2016). Rho GTPases: regulation and roles in cancer cell biology. Small GTPases 7, 207–221. [PubMed: 27628050]

Hernández AJA, Reyes VL, Albores-García D, Gómez R, and Calderón-Aranda ES (2018). MeHg affects the activation of FAK, Src, Rac1 and Cdc42, critical proteins for cell movement in PDGF-stimulated SH-SY5Y neuroblastoma cells. Toxicology 394, 35–44. [PubMed: 29197552]

Hirano T, Shinsato Y, Tanabe K, Higa N, Kamil M, Kawahara K, Yamamoto M, Minami K, Shimokawa M, Arigami T, et al. (2020). FARP1 boosts CDC42 activity from integrin αvβ5

signaling and correlates with poor prognosis of advanced gastric cancer. Oncogenesis 9, 13. [PubMed: 32029704]

Hodge RG, Schaefer A, Howard SV, and Der CJ (2020). RAS and RHO family GTPase mutations in cancer: twin sons of different mothers? Crit. Rev. Biochem. Mol. Biol 55, 386–407. [PubMed: 32838579]

Innocenti M (2018). New insights into the formation and the function of lamellipodia and ruffles in mesenchymal cell migration. Cell Adhes. Migr 12, 401–416.

Ishikawa M, Sonobe M, Nakayama E, Kobayashi M, Kikuchi R, Kitamura J, Imamura N, and Date H (2013). Higher expression of receptor tyrosine kinase Axl, and differential expression of its ligand, Gas6, predict poor survival in lung adenocarcinoma patients. Ann. Surg. Oncol 20 (Suppl 3), S467–S476. [PubMed: 23242819]

Justilien V, Ali SA, Jamieson L, Yin N, Cox AD, Der CJ, Murray NR, and Fields AP (2017). Ect2-dependent rRNA synthesis is required for KRAS-TRP53-driven lung adenocarcinoma. Cancer Cell 31, 256–269. [PubMed: 28110998]

Kallin A, Demoulin JB, Nishida K, Hirano T, Rönnstrand L, and Heldin CH (2004). Gab1 contributes to cytoskeletal reorganization and chemotaxis in response to platelet-derived growth factor. J. Biol. Chem 279, 17897–17904. [PubMed: 14973141]

Kanzaki R, Naito H, Kise K, Takara K, Eino D, Minami M, Shintani Y, Funaki S, Kawamura T, Kimura T, et al. (2017). Gas6 derived from cancer-associated fibroblasts promotes migration of Axl-expressing lung cancer cells during chemotherapy. Sci. Rep 7, 10613. [PubMed: 28878389]

Kazanietz MG, and Caloca MJ (2017). The Rac GTPase in cancer: from old concepts to new paradigms. Cancer Res. 77, 5445–5451. [PubMed: 28807941]

Kharbanda A, Walter DM, Gudiel AA, Schek N, Feldser DM, and Witze ES (2020). Blocking EGFR palmitoylation suppresses PI3K signaling and mutant KRAS lung tumorigenesis. Sci. Signal 13, aax2364.

Kim J, Jang SJ, Choi CM, and Ro JY (2016). Correlation of histologic subtypes and molecular alterations in pulmonary adenocarcinoma: therapeutic and prognostic implications. Adv. Anat. Pathol 23, 330–338. [PubMed: 27403614]

Kissil JL, Walmsley MJ, Hanlon L, Haigis KM, Bender Kim CF, Sweet-Cordero A, Eckman MS, Tuveson DA, Capobianco AJ, Tybulewicz VL, and Jacks T (2007). Requirement for Rac1 in a K-ras induced lung cancer in the mouse. Cancer Res. 67, 8089–8094. [PubMed: 17804720]

Kondo A, Hirayama N, Sugito Y, Shono M, Tanaka T, and Kitamura N (2008). Coupling of Grb2 to Gab1 mediates hepatocyte growth factor-induced high intensity ERK signal required for inhibition of HepG2 hepatoma cell proliferation. J. Biol. Chem 283, 1428–1436. [PubMed: 18003605]

Kruspig B, Monteverde T, Neidler S, Hock A, Kerr E, Nixon C, Clark W, Hedley A, Laing S, Coffelt SB, et al. (2018). The ERBB network facilitates KRAS-driven lung tumorigenesis. Sci. Transl. Med 10, eaao2565. [PubMed: 29925636]

Kuo YC, He X, Coleman AJ, Chen YJ, Dasari P, Liou J, Biederer T, and Zhang X (2018). Structural analyses of FERM domain-mediated membrane localization of FARP1. Sci. Rep 8, 10477. [PubMed: 29992992]

Lawson CD, and Ridley AJ (2018). Rho GTPase signaling complexes in cell migration and invasion. J. Cell Biol 217, 447–457. [PubMed: 29233866]

Levin PA, Brekken RA, Byers LA, Heymach JV, and Gerber DE (2016). Axl receptor axis: a new therapeutic target in lung cancer. J. Thorac. Oncol 11, 1357–1362. [PubMed: 27130831]

Li W, Xiong X, Abdalla A, Alejo S, Zhu L, Lu F, and Sun H (2018). HGF-induced formation of the MET-AXL-ELMO2-DOCK180 complex promotes RAC1 activation, receptor clustering, and cancer cell migration and invasion. J. Biol. Chem 293, 15397–15418. [PubMed: 30108175]

Lim W, Ridge CA, Nicholson AG, and Mirsadraee S (2018). The 8th lung cancer TNM classification and clinical staging system: review of the changes and clinical implications. Quant. Imaging Med. Surg 8, 709–718. [PubMed: 30211037]

Lock LS, Royal I, Naujokas MA, and Park M (2000). Identification of an atypical Grb2 carboxyl-terminal SH3 domain binding site in Gab docking proteins reveals Grb2-dependent and -independent recruitment of Gab1 to receptor tyrosine kinases. J. Biol. Chem 275, 31536–31545. [PubMed: 10913131]

Maldonado MDM, and Dharmawardhane S (2018). Targeting Rac and Cdc42 GTPases in Cancer. Cancer Res. 78, 3101–3111. [PubMed: 29858187]

Maltas J, Reed H, Porter A, and Malliri A (2020). Mechanisms and consequences of dysregulation of the Tiam family of Rac activators in disease. Biochem. Soc. Trans 48, 2703–2719. [PubMed: 33200195]

Marei H, and Malliri A (2017). Rac1 in human diseases: the therapeutic potential of targeting Rac1 signaling regulatory mechanisms. Small GTPases 8, 139–163. [PubMed: 27442895]

Meller J, Vidali L, and Schwartz MA (2008). Endogenous RhoG is dispensable for integrin-mediated cell spreading but contributes to Rac-independent migration. J. Cell Sci 121, 1981–1989. [PubMed: 18505794]

Meyer AS, Miller MA, Gertler FB, and Lauffenburger DA (2013). The receptor AXL diversifies EGFR signaling and limits the response to EGFR-targeted inhibitors in triple-negative breast cancer cells. Sci. Signal 6, ra66. [PubMed: 23921085]

Moll HP, Pranz K, Musteanu M, Grabner B, Hruschka N, Mohrherr J, Aigner P, Stiedl P, Brcic L, Laszlo V, et al. (2018). Afatinib restrains KRAS-driven lung tumorigenesis. Sci. Transl. Med 10, eaao2301. [PubMed: 29925635]

Müller PM, Rademacher J, Bagshaw RD, Wortmann C, Barth C, van Unen J, Alp KM, Giudice G, Eccles RL, Heinrich LE, et al. (2020). Systems analysis of RhoGEF and RhoGAP regulatory proteins reveals spatially organized RAC1 signalling from integrin adhesions. Nat. Cell Biol 22, 498–511. [PubMed: 32203420]

Oberndorfer F, and Müllauer L (2018). Molecular pathology of lung cancer: current status and perspectives. Curr. Opin. Oncol 30, 69–76. [PubMed: 29251665]

Olson MF, and Sahai E (2009). The actin cytoskeleton in cancer cell motility. Clin. Exp. Metastasis 26, 273–287. [PubMed: 18498004]

Quatromoni JG, Singhal S, Bhojnagarwala P, Hancock WW, Albelda SM, and Eruslanov E (2015). An optimized disaggregation method for human lung tumors that preserves the phenotype and function of the immune cells. J. Leukoc. Biol 97, 201–209. [PubMed: 25359999]

Radu M, Semenova G, Kosoff R, and Chernoff J (2014). PAK signalling during the development and progression of cancer. Nat. Rev. Cancer 14, 13–25. [PubMed: 24505617]

Reddy RJ, Gajadhar AS, Swenson EJ, Rothenberg DA, Curran TG, and White FM (2016). Early signaling dynamics of the epidermal growth factor receptor. Proc. Natl. Acad. Sci. USA 113, 3114–3119. [PubMed: 26929352]

Riihimäki M, Hemminki A, Fallah M, Thomsen H, Sundquist K, Sundquist J, and Hemminki K (2014). Metastatic sites and survival in lung cancer. Lung Cancer 86, 78–84. [PubMed: 25130083]

Roskoski R Jr. (2014). The ErbB/HER family of protein-tyrosine kinases and cancer. Pharmacol. Res 79, 34–74. [PubMed: 24269963]

Rossman KL, Der CJ, and Sondek J (2005). GEF means go: turning on RHO GTPases with guanine nucleotide-exchange factors. Nat. Rev. Mol. Cell Biol 6, 167–180. [PubMed: 15688002]

Sampaio C, Dance M, Montagner A, Edouard T, Malet N, Perret B, Yart A, Salles JP, and Raynal P (2008). Signal strength dictates phosphoinositide 3-kinase contribution to Ras/extracellular signal-regulated kinase 1 and 2 activation via differential Gab1/Shp2 recruitment: consequences for resistance to epidermal growth factor receptor inhibition. Mol. Cell. Biol 28, 587–600. [PubMed: 18025104]

Scheffler M, Ihle MA, Hein R, Merkelbach-Bruse S, Scheel AH, Siemanowski J, Brägelmann J, Kron A, Abedpour N, Ueckeroth F, et al. (2019). K-ras mutation subtypes in NSCLC and associated co-occuring mutations in other oncogenic pathways. J. Thorac. Oncol 14, 606–616. [PubMed: 30605727]

Shepherd TR, Hard RL, Murray AM, Pei D, and Fuentes EJ (2011). Distinct ligand specificity of the Tiam1 and Tiam2 PDZ domains. Biochemistry 50, 1296–1308. [PubMed: 21192692]

Sosa MS, Lopez-Haber C, Yang C, Wang H, Lemmon MA, Busillo JM, Luo J, Benovic JL, Klein-Szanto A, Yagi H, et al. (2010). Identification of the Rac-GEF P-Rex1 as an essential mediator of ErbB signaling in breast cancer. Mol. Cell 40, 877–892. [PubMed: 21172654]

Suda K, Tomizawa K, and Mitsudomi T (2010). Biological and clinical significance of KRAS mutations in lung cancer: an oncogenic driver that contrasts with EGFR mutation. Cancer Metastasis Rev. 29, 49–60. [PubMed: 20108024]

Suzawa K, Offin M, Lu D, Kurzatkowski C, Vojnic M, Smith RS, Sabari JK, Tai H, Mattar M, Khodos I, et al. (2019). Activation of KRAS mediates resistance to targeted therapy in MET exon 14-mutant non-small cell lung cancer. Clin. Cancer Res 25, 1248–1260. [PubMed: 30352902]

Timmerman I, Heemskerk N, Kroon J, Schaefer A, van Rijssel J, Hoogenboezem M, van Unen J, Goedhart J, Gadella TW Jr., Yin T, et al. (2015). A local VE-cadherin and Trio-based signaling complex stabilizes endothelial junctions through Rac1. J. Cell Sci 128, 3041–3054. [PubMed: 26116572]

Trusolino L, Bertotti A, and Comoglio PM (2010). MET signalling: principles and functions in development, organ regeneration and cancer. Nat. Rev. Mol. Cell Biol 11, 834–848. [PubMed: 21102609]

Valdivia A, Goicoechea SM, Awadia S, Zinn A, and Garcia-Mata R (2017). Regulation of circular dorsal ruffles, macropinocytosis, and cell migration by RhoG and its exchange factor, Trio. Mol. Biol. Cell 28, 1768–1781. [PubMed: 28468978]

Watanabe T, Tsuda M, Makino Y, Ichihara S, Sawa H, Minami A, Mochizuki N, Nagashima K, and Tanaka S (2006). Adaptor molecule Crk is required for sustained phosphorylation of Grb2-associated binder 1 and hepatocyte growth factor-induced cell motility of human synovial sarcoma cell lines. Mol. Cancer Res 4, 499–510. [PubMed: 16849525]

Woroniuk A, Porter A, White G, Newman DT, Diamantopoulou Z, Waring T, Rooney C, Strathdee D, Marston DJ, Hahn KM, et al. (2018). STEF/TIAM2-mediated Rac1 activity at the nuclear envelope regulates the perinuclear actin cap. Nat. Commun 9, 2124. [PubMed: 29844364]

Yang C, Liu Y, Lemmon MA, and Kazanietz MG (2006). Essential role for Rac in heregulin beta1 mitogenic signaling: a mechanism that involves epidermal growth factor receptor and is independent of ErbB4. Mol. Cell. Biol 26, 831–842. [PubMed: 16428439]

Yang H, Liang SQ, Xu D, Yang Z, Marti TM, Gao Y, Kocher GJ, Zhao H, Schmid RA, and Peng RW (2019). HSP90/AXL/eIF4E-regulated unfolded protein response as an acquired vulnerability in drug-resistant KRAS-mutant lung cancer. Oncogenesis 8, 45. [PubMed: 31431614]

Yohe ME, Rossman K, and Sondek J (2008). Role of the C-terminal SH3 domain and N-terminal tyrosine phosphorylation in regulation of Tim and related Dbl-family proteins. Biochemistry 47, 6827–6839. [PubMed: 18537266]

Yu B, Martins IR, Li P, Amarasinghe GK, Umetani J, Fernandez-Zapico ME, Billadeau DD, Machius M, Tomchick DR, and Rosen MK (2010). Structural and energetic mechanisms of cooperative autoinhibition and activation of Vav1. Cell 140, 246–256. [PubMed: 20141838]

Zhao ZY, Han CG, Liu JT, Wang CL, Wang Y, and Cheng LY (2013). TIAM2 enhances non-small cell lung cancer cell invasion and motility. Asian Pac. J. Cancer Prev 14, 6305–6309. [PubMed: 24377522]

Zhou H, Cai L, Zhang X, Li A, Miao Y, Li Q, Qiu X, and Wang E (2018). ARHGEF39 promotes tumor progression via activation of Rac1/P38 MAPK/ATF2 signaling and predicts poor prognosis in non-small cell lung cancer patients. Lab. Invest 98, 670–681. [PubMed: 29382922]

Highlights

- FARP1, ARHGEF39, and TIAM2 drive motility signaling in lung adenocarcinoma cells
- These Rac-GEFs act as effectors of EGFR, c-MET, and AXL receptor tyrosine kinases
- Their functional non-redundancy relates to unique effects on ruffle dynamics
- FARP1 and ARHGEF39 are upregulated in $EpCam^{+}$ cells sorted from human lung tumors

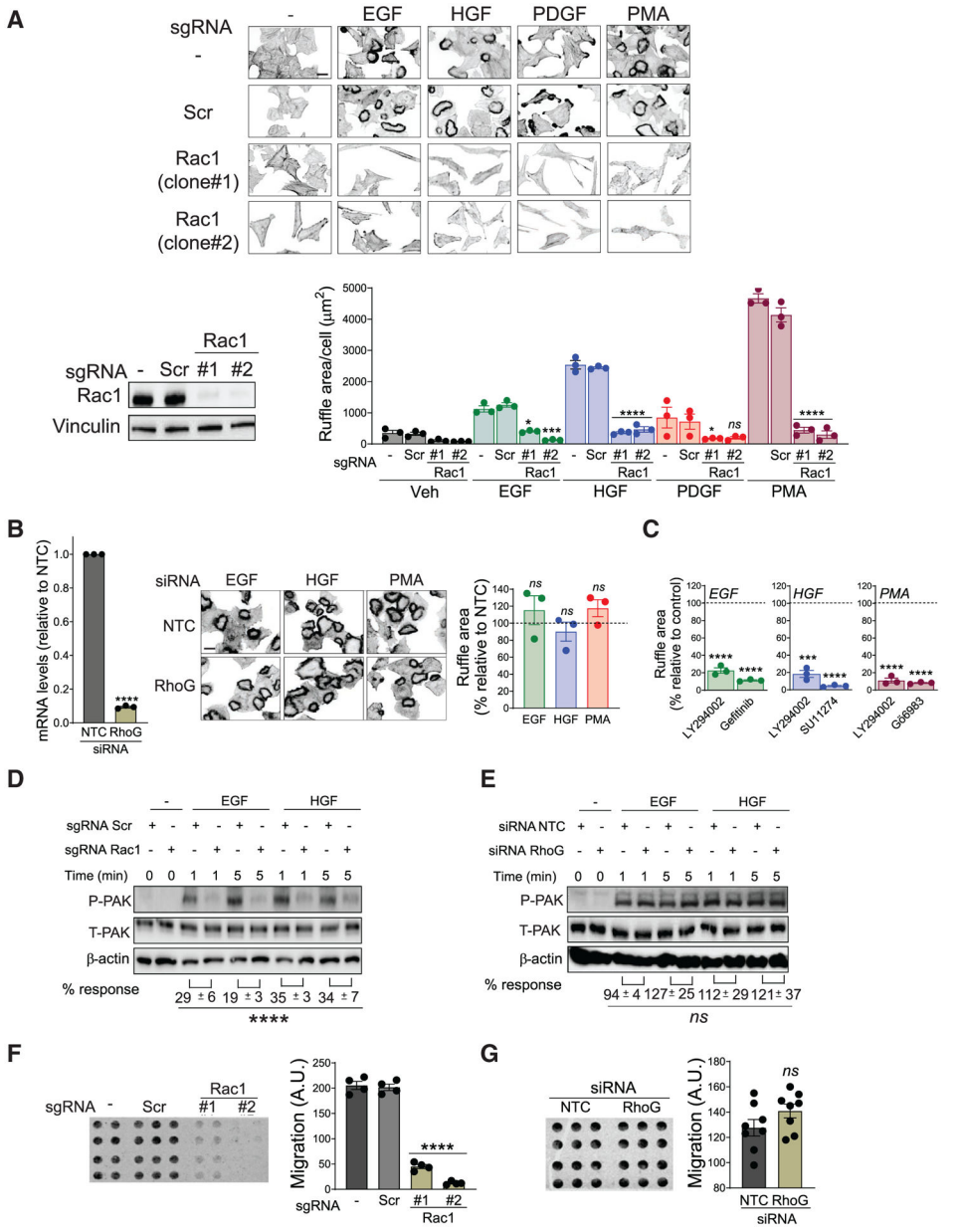

Figure 1. Rac1-dependent, RhoG-independent growth factor-induced ruffle formation in lung adenocarcinoma cells

(A) A549 cells subjected to Rac1 CRISPR/Cas9 KO (clones 1 and 2) or scrambled CRISPR control cells (*Scr*) were stimulated with EGF (100 ng/mL, 5 min), HGF (100 ng/mL, 15 min), PDGF (100 ng/mL, 15 min), or PMA (100 nM, 30 min), fixed, and stained with rhodamine phalloidin. Upper, representative micrographs. Lower left, expression of Rac1 by western blot. Lower right, quantification of ruffle formation using ImageJ. Results are expressed as means ± SEMs of 3 individual experiments. *p < 0.05; ****p < 0.0001 versus single-guide RNA (sgRNA); ns, not significant. Scale bar, 10 μm.

(B) Effect of RhoG RNAi silencing on growth factor-induced ruffle formation. Left, RhoG mRNA levels in RhoG-depleted cells, relative to non-target control (NTC). Center, representative micrographs of rhodamine-phalloidin stained cells. Right, quantification of

ruffle formation. Results (means ± SEMs, n = 3) are expressed as percentage relative to NTC (dotted line). Scale bar, 10 μm.

(C) Effect of LY294002 (PI3K inhibitor 20 μM), gefitinib (EGFR inhibitor, 3 μM), SU11247 (c-Met inhibitor, 5 μM), or Gö6983 (PKC inhibitor, 3 μM) on ruffle formation induced by EGF, HGF, or PMA. Results (means ± SEMs, n = 3) are expressed as percentage of response in the absence of inhibitor (dotted line). ***p < 0.001; ****p < 0.0001 versus no inhibitor.

(D) Phospho-PAK levels in response to growth factor stimulation. A representative western blot and densitometric analysis of 3 independent experiments, normalized to β-actin (means ± SEMs, n = 3) is shown; ****p < 0.0001 versus sgRNA.

(E) Phospho-PAK levels in A549 cells subjected to RhoG or NTC RNAi in response to growth factors. A representative western blot and densitometric analysis of 3 independent experiments, normalized to β-actin (means ± SEMs, n = 3), is shown; ns, not significant versus NTC.

(F) Migration of Rac1 KO A549 and control (*Scr*) cells as determined with a Boyden chamber. Left, representative experiment. Right, quantification of migratory cells. Results were expressed as means ± SEMs of 4 individual experiments. ****p < 0.0001 versus parental.

(G) Migration of A549 cells subjected to RhoG or NTC RNAi. Left, representative experiment. Right, quantification of migratory cells. Results were expressed as means ± SEMs of 8 individual experiments. ns, not significant versus NTC.

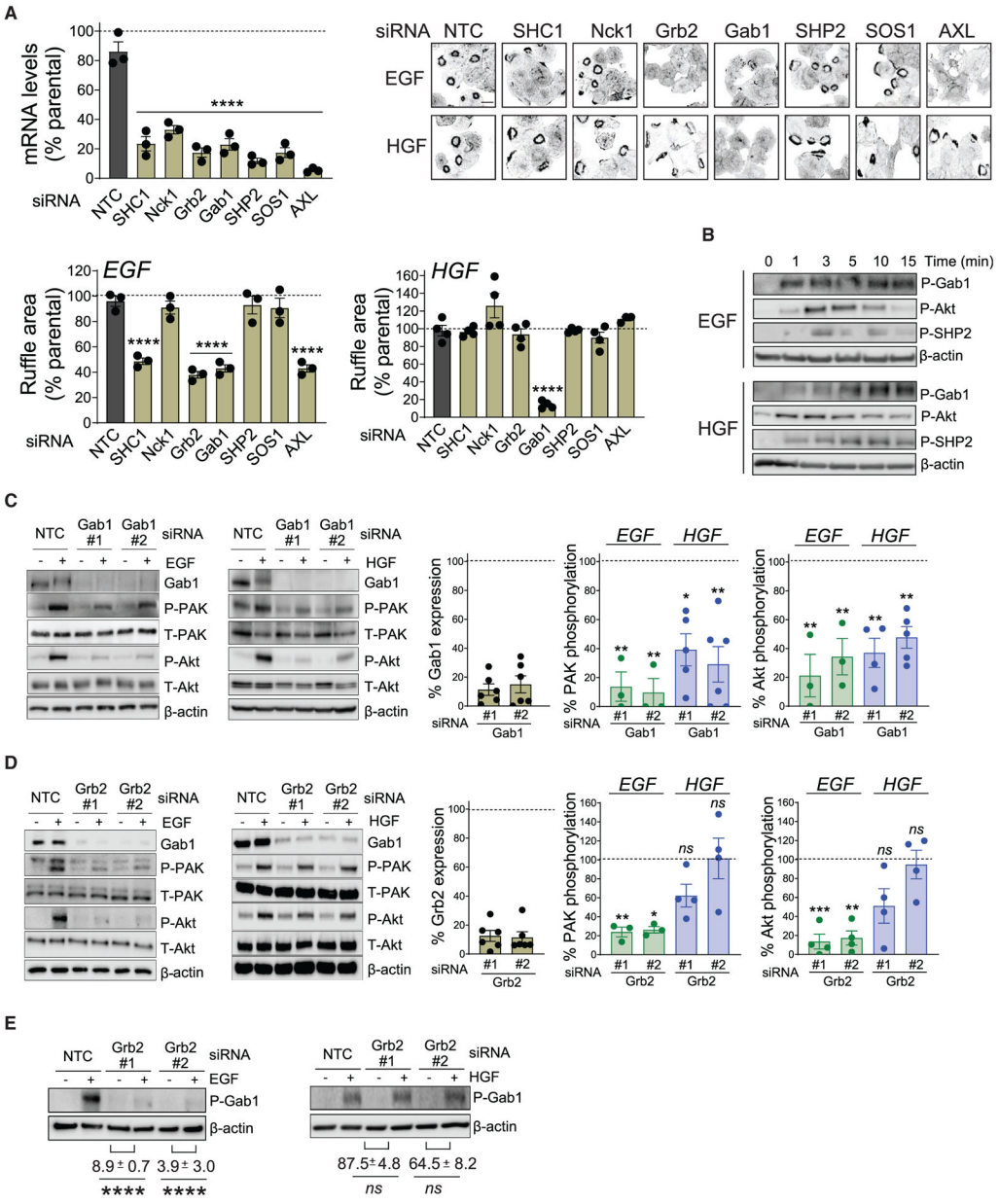

Figure 2. Adaptor and effector dependency for ruffle formation in response to EGF and HGF

(A) A549 was transfected with the indicated siRNA duplexes. After 48 h, cells were serum starved and treated with either EGF (100 ng/mL, 5 min) or HGF (100 ng/mL, 15 min). Upper left, mRNA levels relative to parental cells (dotted line). Upper right, representative micrographs of rhodamine-phalloidin stained cells. Lower, quantification of ruffle area in response to EGF or HGF, relative to parental cell (dotted line). Results are expressed as means ± SEMs (n = 3). ****p < 0.0001 versus NTC. Scale bar, 10 μM.

(B) Time course analysis of phosphorylated Gab1, Akt, and SHP2 in response to EGF or HGF.

(C) Effect of Gab1 RNAi on signaling in response to EGF or HGF.

(D) Effect of Grb2 RNAi on signaling in response to EGF or HGF.

(E) Effect of Grb2 RNAi on Gab1 phosphorylation by EGF or HGF.

For (C)–(E), representative western blots are shown with the corresponding densitometric analysis of 3 independent experiments. Results (means ± SEMs) are expressed as percentage relative to the corresponding activation in NTC cells. **p < 0.01; ***p < 0.001; ****p < 0.0001; ns, not significant versus NTC.

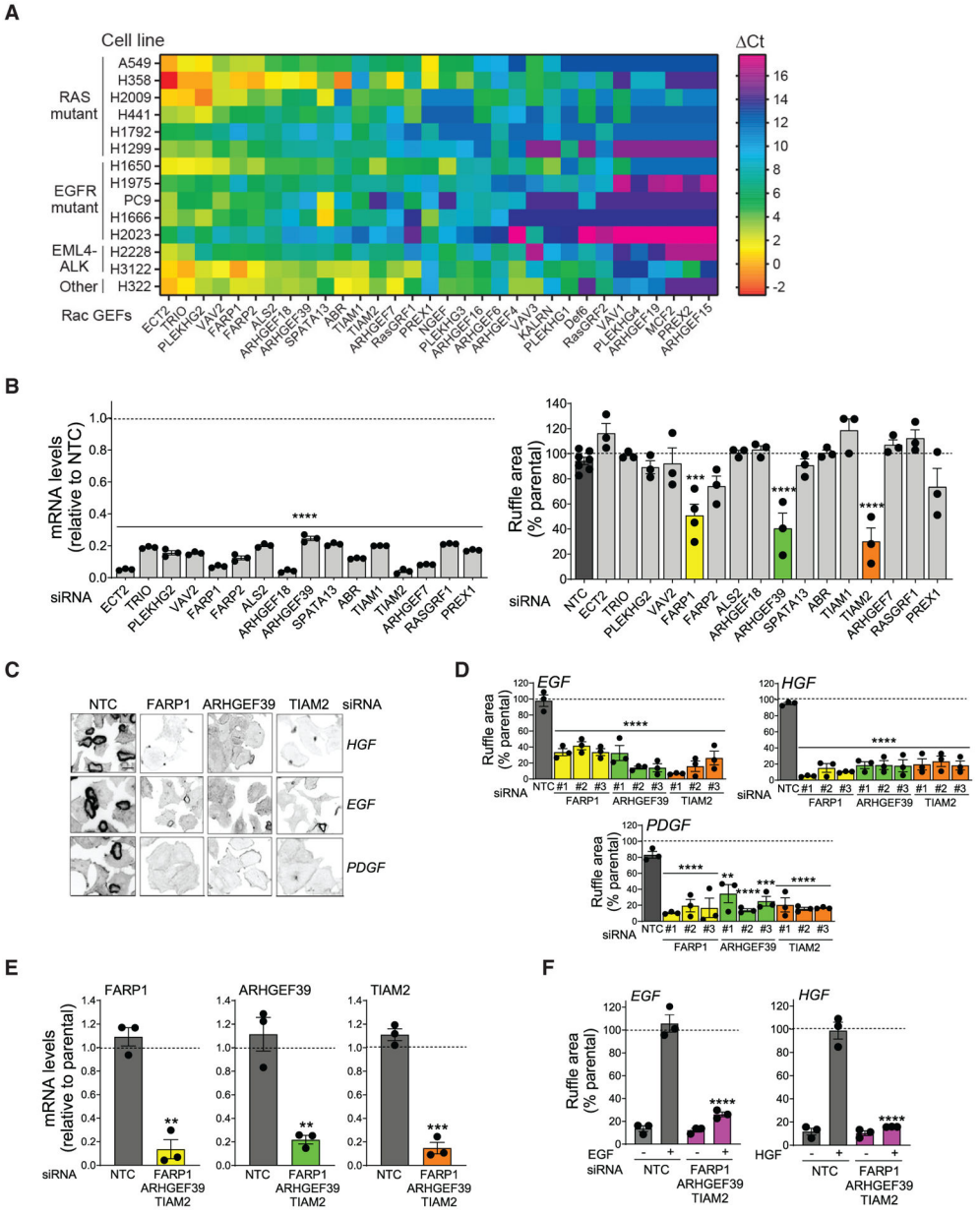

Figure 3. Identification of Rac-GEFs mediating ruffle formation in lung adenocarcinoma cells

(A) Heatmap for Rac-GEF expression according to the qPCR array in lung adenocarcinoma cell lines with different genetic alterations, as determined with a Rac-GEF qPCR array. Expression is shown as ΔCt for each Rac-GEF relative to the average of UBC and B2M housekeeping genes.

(B) A549 was transfected with the indicated siRNA duplexes. After 48 h, cells were serum starved and treated with HGF (100 ng/mL, 15 min). Left, mRNA levels for each Rac-GEF relative to NTC (dotted line). Right, quantification of ruffle formation. Results (means ± SEMs) are expressed as percentage relative to parental (dotted line). ***p < 0.001; ****p < 0.0001 versus NTC.

(C) Representative micrographs of rhodamine-phalloidin-stained cells (NTC and siRNA#1 for each Rac-GEF). Scale bar, 10 μm.
(D) Effect of silencing FARP1, ARHGEF39, or TIAM2 with 3 different siRNA duplexes. Results (means ± SEMs, n = 3) are expressed as percentage of ruffles formed in parental cells (dotted line). **p < 0.01; ***p < 0.001; ****; p < 0.0001 versus NTC.
(E) Simultaneous FARP1, ARHGEF39, and TIAM2 triple knockdown in A549 cells. mRNA levels for the indicated Rac-GEFs are expressed as relative to parental cells (dotted line). Results are expressed as means ± SEMs (n = 3) relative to parental cells (dotted line). **p < 0.01; ***p < 0.001.
(F) Effect of triple Rac-GEF knockdown on ruffle formation induced by EGF (left) or HGF (right). Results (means ± SEMs, n = 3) are expressed as percentage response relative to parental cells treated with the corresponding growth factor (dotted line). ****p < 0.0001 versus NTC.

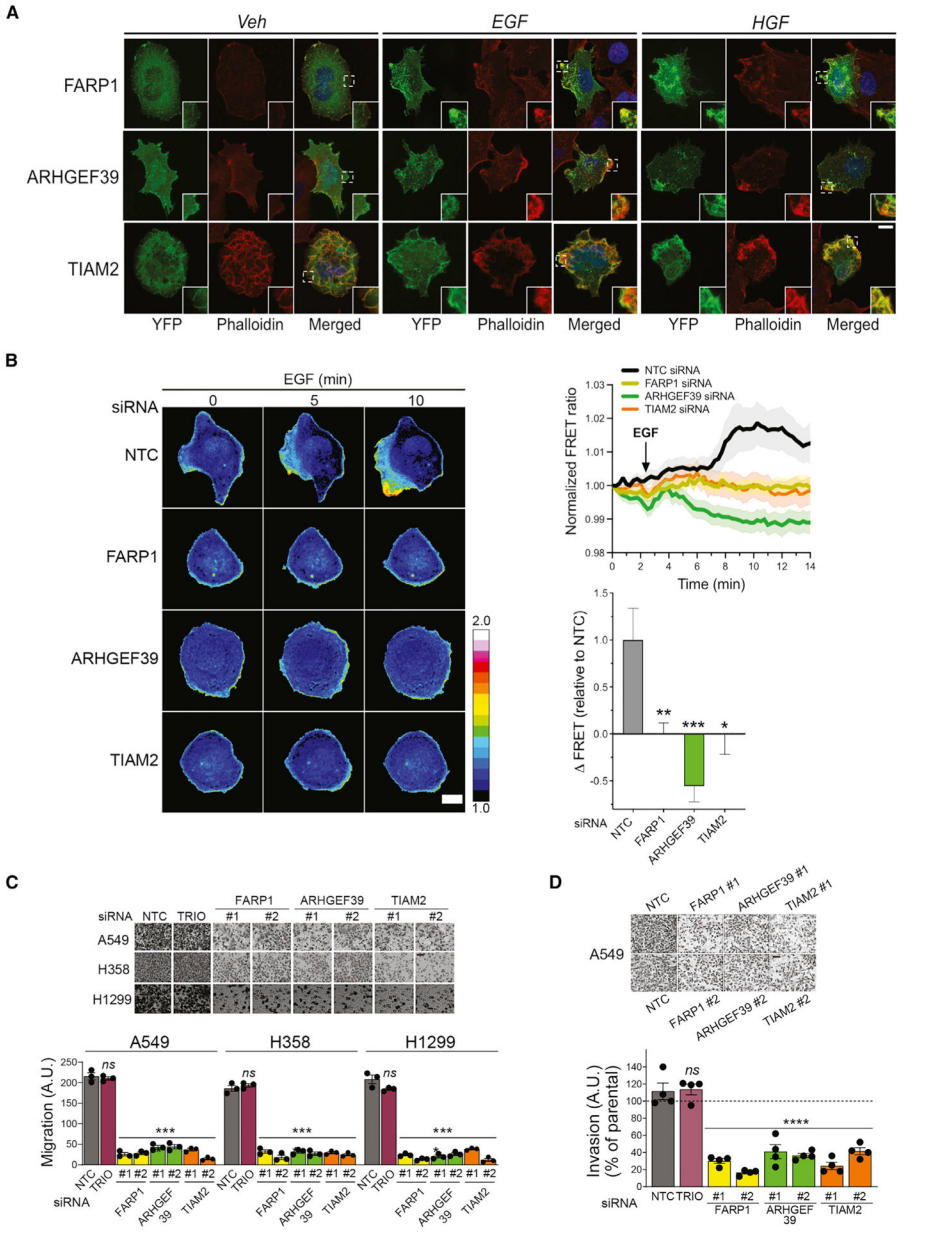

Figure 4. FARP1, AHRGEF39, and TIAM2 are required for Rac1 activation in cell ruffles, cell motility, and invasion

(A) Localization of YFP-tagged Rac-GEFs in vehicle versus EGF- or HGF-treated A549 cells (100 ng/mL) as determined by confocal microscopy. Insets, enlarged images of selected regions. Scale bar, 10 μm.

(B) Left, A549 cells stably expressing the Rac1 biosensor were starved overnight, treated with 100 ng/mL EFG, and imaged live every 15 s for Venus/Cerulean. Left, representative images show Rac1 activation in cells subjected to RNAi for each Rac-GEF or NTC RNAi. Color scale bar, dynamic range of the biosensor response (1.0, no significant response; 2.0, strongest response throughout the time-lapse sequence). Top right, quantification of the ratiometric changes in NTC versus Rac-GEF-depleted cells. The graph shows data from 3 independent experiments (n ≥ 30 cells for each condition) expressed as means ± SEMs.

Bottom right, changes in FRET ratios induced by EGF (relative to NTC) were graphed for each condition at the maximum time of Rac1 activation in NTC cells. Scale bar, 10 μm.
(C) A549, H358, or H1299 cells were transfected with the indicated Rac-GEF siRNA duplexes. After 48 h, cells were subjected to a Boyden chamber migration assay. Upper, representative micrographs. Lower, quantification of migratory cells after counting in 5 random fields by contrast microscopy. Results are expressed as means ± SEMs of 3 independent experiments. ****$p < 0.0001$ versus NTC. Scale bar, 50 μm.
(D) Boyden chamber invasion assay through Matrigel, 48 h after transfection with the indicated Rac-GEF siRNA duplexes. Upper, representative micrographs. Lower, quantification. Results were normalized to invasion of parental cells and expressed as means ± SEMs of 4 independent experiments. ****$p < 0.0001$ versus NTC. Scale bar, 50 μm.

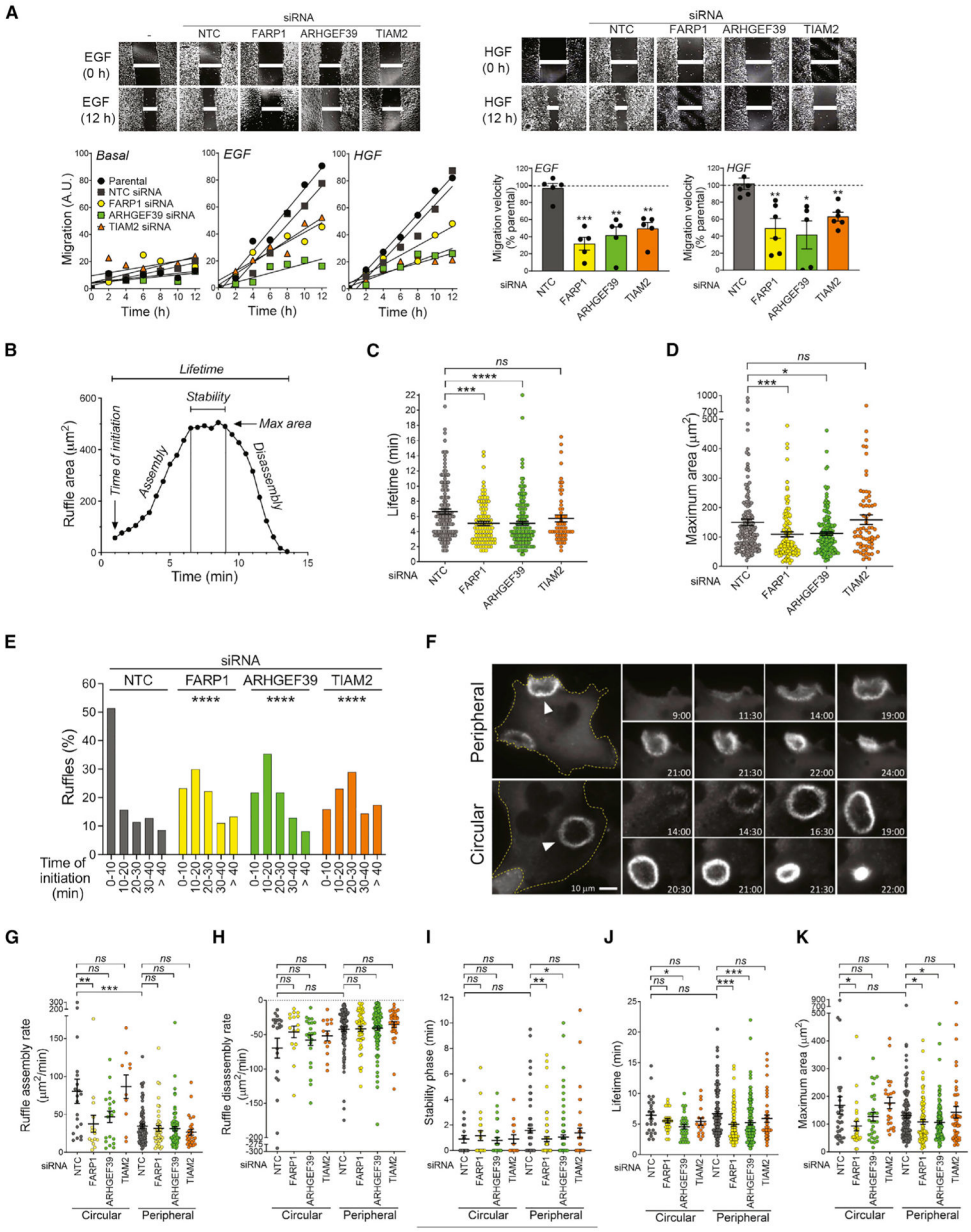

Figure 5. Involvement of FARP1, ARHGEF39, and TIAM2 in growth factor-induced motility and ruffle formation dynamics

(A) A549 cells were transfected with the indicated Rac-GEF siRNA duplexes and 48 h later serum starved for 16 h. Cell motility was determined using a quantitative wound assay. Upper, representative wound micrographs in A549 cells at 0 and 12 h after addition of EGF (left) or HGF (right) (100 ng/mL). White line, wound. Lower left, representative migration curves. Lower right, migration velocity of Rac-GEF depleted A549 cells, relative to parental cells. Results are expressed as means ± SEMs of 5 independent experiments. *p < 0.05; **p < 0.01; ***p < 0.001 versus NTC. Dotted line, parental cells. Scale bar, 250 μm.

(B) FARP1, ARHGEF39, or TIAM2 KD A549 cells expressing mCherry-cortactin were serum starved and imaged before and after stimulation with EGF (100 ng/mL) and subjected to analysis of ruffle formation. Results were expressed as means ± SEMs from at least 3

independent experiments (n = 150, 102, 158, and 68 for NTC, FARP1 KD, ARHGEF39 KD, and TIAM2 KD, respectively). The graph shows the variables analyzed for ruffle formation after addition of stimulus.

(C) Total ruffle lifetime (min).

(D) Total ruffle maximum area (μm^2).

(E) Percentage of total ruffles formed at different times after stimulation (distribution frequencies analyzed by chi-square test).

(F) A549 cells expressing mCherry-cortactin were plated on glass bottom dishes, serum starved, and imaged live before and after treatment with EGF (100 ng/mL). Left, representative examples of peripheral and circular ruffles (white arrowheads). Yellow dashed lines highlight the edge of the cell. Right, individual time points covering the entire life cycle of a peripheral ruffle and a circular ruffle. Scale bar, 10 μm.

(G) Circular and peripheral ruffle assembly rate ($\mu m^2 \times min^{-1}$).

(H) Circular and peripheral ruffle disassembly rate ($\mu m^2 \times min^{-1}$).

(I) Circular and peripheral ruffle stability (min).

(J) Circular and peripheral ruffle lifetime (min).

(K) Circular and peripheral maximum area (μm^2).

For (C), (D), and (G)–(K), results are expressed as means ± SEMs (n = 68–158). *$p < 0.05$; **$p < 0.01$; ***$p < 0.001$; ****$p < 0.0001$; ns, not significant.

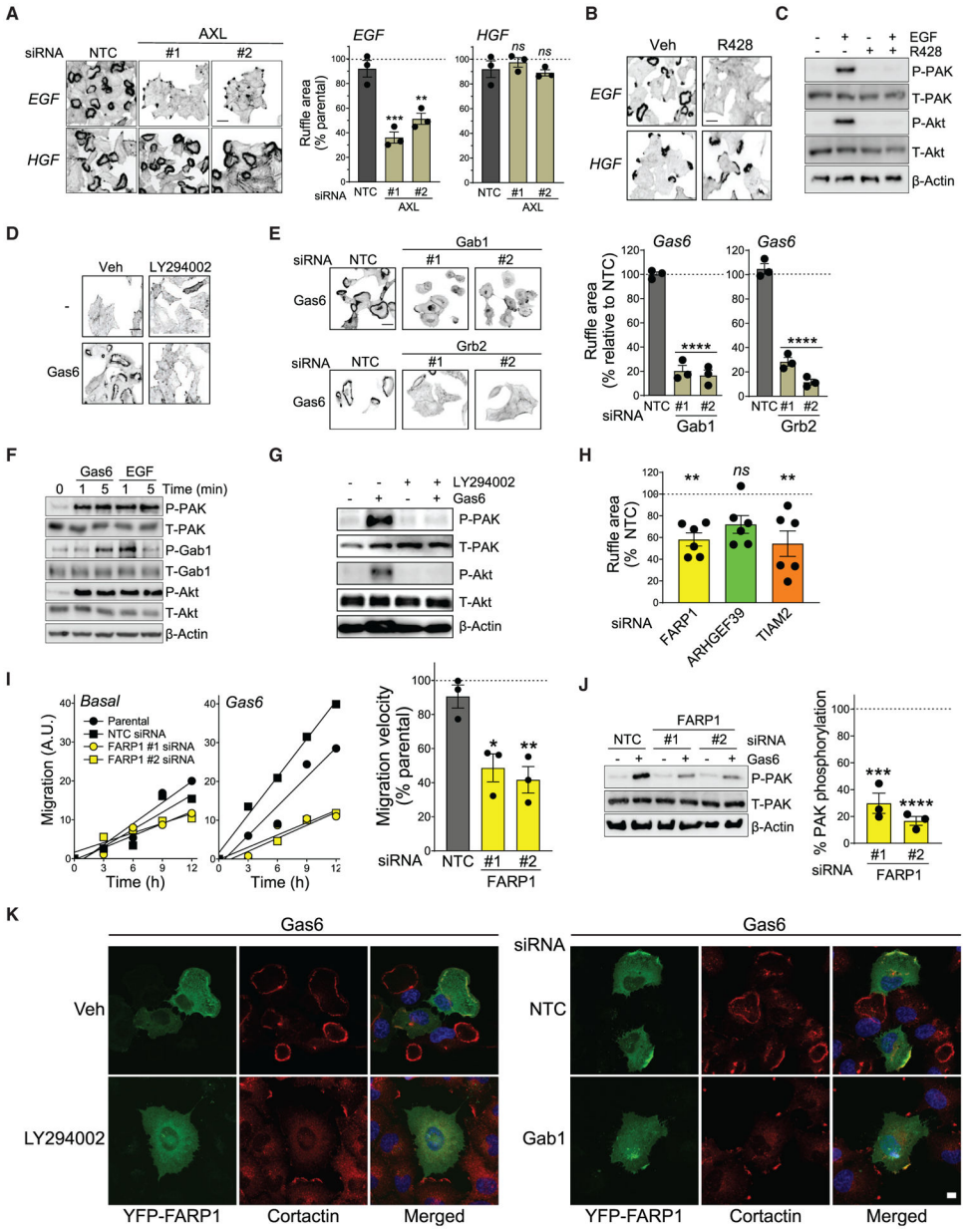

Figure 6. AXL is required for EGF-mediated motility signaling in lung adenocarcinoma cells

(A) A549 were transfected with AXL siRNA duplexes. After 48 h, cells were serum starved and treated with either EGF (100 ng/mL, 5 min) or HGF (100 ng/mL, 15 min). Left, representative micrographs of rhodamine-phalloidin-stained cells. Right, quantification of ruffle area in response to EGF or HGF, relative to parental cells (dotted line). Results are expressed as means ± SEMs (n = 3). **p < 0.01; ***p < 0.001; ns, not significant versus NTC. Scale bar, 10 μm.

(B) Effect of R428 (5 μM) on ruffle formation induced by EGF or HGF. Scale bar, 10 μm.

(C) Analysis for phospho- and total PAK and Akt in EGF-stimulated A549 cells treated with R428.

(D) Effect of the PI3K inhibitor LY294002 (20 μM, 1 h) on ruffle formation induced by Gas6 (200 ng/mL, 15 min) in H1299 cells. Scale bar, 10 μm.
(E) Effect of Gab1 and Grb2 RNAi on Gas6-induced ruffle formation. Left, representative micrographs. Right, quantification of ruffle formation. Results (means ± SEMs) are expressed as percentage relative to NTC cells. ****$p < 0.0001$ versus NTC, Gas6-treated cells. Dotted line, parental cells. Scale bar, 10 μm.
(F) PAK, Gab1, and Akt activation by Gas6 in H1299 cells. Representative western blots are shown.
(G) Effect of LY294002 on PAK and Akt activation by Gas6 (200 ng/mL, 5 min).
(H) Ruffle formation by Gas6 in the indicated Rac-GEF KD A549 cells. Results (means ± SEMs) are expressed percentage relative to NTC cells (dotted line). **$p < 0.01$; ns, not significant versus NTC, Gas6-treated cells.
(I) H1299 cells (parental or transfected with siRNA duplexes for FARP1 or NTC, 48 h) were serum starved for 16 h and motility in response to Gas6 assessed using a quantitative wound assay. Left, representative migration curves. Right, migration velocity of FARP1 depleted A549 cells. Results are expressed as means ± SEMs of 3 independent experiments. *$p < 0.05$; **; $p < 0.01$; versus NTC. Dotted line, parental cells.
(J) Effect of FARP1 RNAi on PAK activation. Left, representative western blots; right, densitometric analysis, normalized to β-actin (means ± SEMs, n = 3). ***$p < 0.001$; ****$p < 0.001$ versus NTC, Gas6-stimulated cells (dotted line).
(K) Localization of YFP-FARP1 in Gas6-treated H1299 cells, as determined by confocal microscopy. Left, effect of the PI3K inhibitor LY294002. Right, effect of Gab1 RNAi. Scale bar, 10 μm.

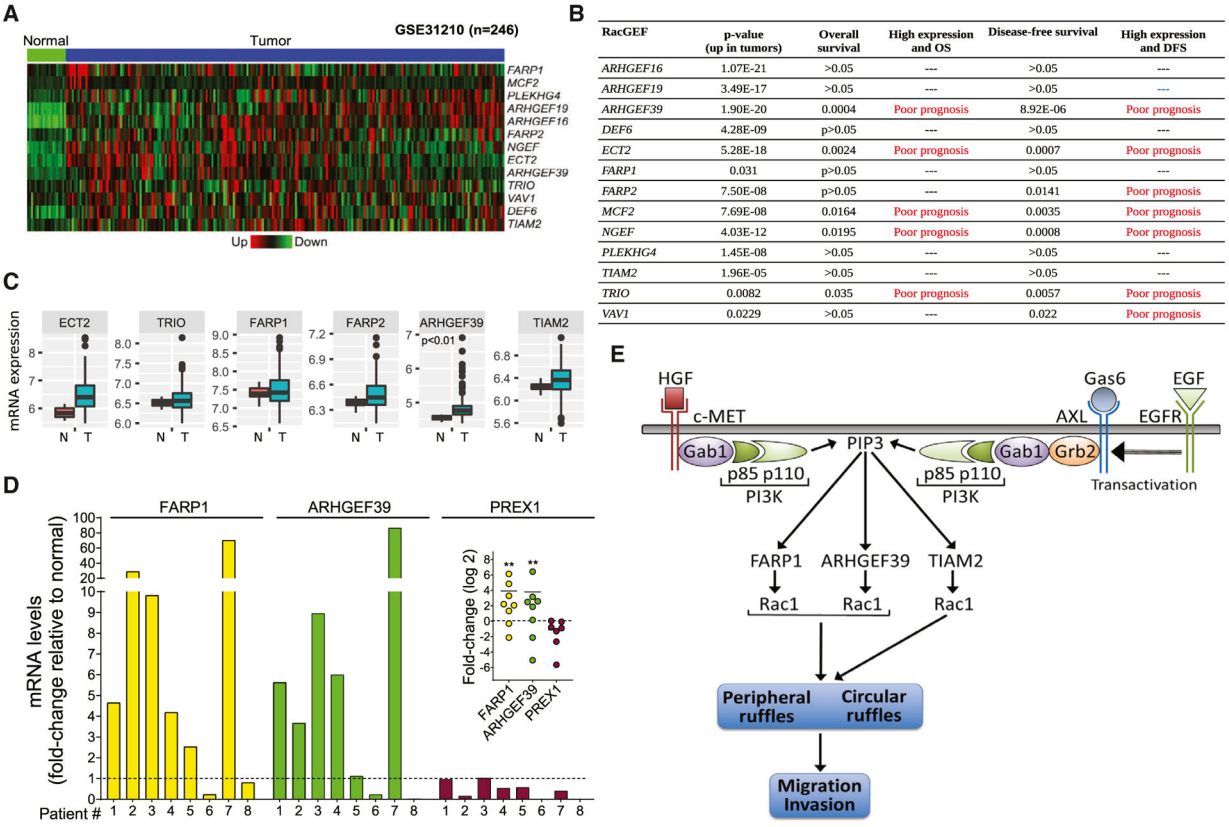

RacGEF	p-value (up in tumors)	Overall survival	High expression and OS	Disease-free survival	High expression and DFS
ARHGEF16	1.07E-21	>0.05	---	>0.05	---
ARHGEF19	3.49E-17	>0.05	---	>0.05	---
ARHGEF39	1.90E-20	0.0004	Poor prognosis	8.92E-06	Poor prognosis
DEF6	4.28E-09	p>0.05	---	>0.05	---
ECT2	5.28E-18	0.0024	Poor prognosis	0.0007	Poor prognosis
FARP1	0.031	p>0.05	---	>0.05	---
FARP2	7.50E-08	p>0.05	---	0.0141	Poor prognosis
MCF2	7.69E-08	0.0164	Poor prognosis	0.0035	Poor prognosis
NGEF	4.03E-12	0.0195	Poor prognosis	0.0008	Poor prognosis
PLEKHG4	1.45E-08	>0.05	---	>0.05	---
TIAM2	1.96E-05	>0.05	---	>0.05	---
TRIO	0.0082	0.035	Poor prognosis	0.0057	Poor prognosis
VAV1	0.0229	>0.05	---	0.022	Poor prognosis

Figure 7. Expression of Rac-GEFs human lung adenocarcinomas

(A) Heatmap for Rac-GEFs upregulated in tumor versus normal (n = 226, GEO: GSE31210 human lung adenocarcinoma dataset).

(B) Upregulated Rac-GEFs. The analysis shows p values (tumor versus normal), overall survival (OS) and disease-free survival (DFS).

(C) Boxplot showing upregulated Rac-GEFs in lung adenocarcinomas among those examined for ruffle formation. N, normal; T, tumor.

(D) qPCR expression analysis for the indicated Rac-GEFs in EpCam^{+} tumor cells purified from human lung adenocarcinomas. Results are expressed as fold change relative to EpCam^{+} cells from the corresponding adjacent normal tissue (dotted line). Inset, log2 representation. **p < 0.01.

(E) Hypothetical model for Rac-GEF involvement in ruffle formation by EGF and HGF in lung adenocarcinoma cells.

KEY RESOURCES TABLE

REAGENT or RESOURCE	SOURCE	IDENTIFIER
Antibodies		
Anti-AKT^{S473}	Cell Signaling Technology	Cat# 4060; RRID:AB_2315049
Anti-AKT	Cell Signaling Technology	Cat# 4691; RRID:AB_915783
Anti-phospho-PAK	Cell Signaling Technology	Cat# 2605; RRID:AB_2160222
Anti-PAK1/2/3	Cell Signaling Technology	Cat# 2604;RRID:AB_2160225
Anti-AXL	Cell Signaling Technology	Cat# 8661; RRID:AB_11217435
Anti-AXL^{Y702}	Cell Signaling Technology	Cat# 5724; RRID:AB_10544794
Anti-Gab1	Cell Signaling Technology	Cat# 3232; RRID:AB_2304999
Anti-Gab1^{Y659}	Cell Signaling Technology	Cat# 12745; RRID:AB_2798014
Anti-Grb2	Cell Signaling Technology	Cat# 3972; RRID:AB_10693935
Anti-SHP2	Cell Signaling Technology	Cat# 3752; RRID:AB_2300607
Anti-Rac1clone 23A8	Millipore Sigma	Cat# 05-389; RRID:AB_309712
Anti-RhoG	Cell Signaling Technology	60370
Anti-β-actin	Millipore Sigma	Cat# A5441; RRID:AB_476744
Anti-cortactin	Santa Cruz	Cat# sc-11408; RRID:AB_2088281
Goat anti-Rabbit IgG (H+L) Cross-Adsorbed Secondary Antibody, Alexa Fluor 594	Invitrogen	Cat# R37117, RRID:AB_2556545
Anti-rabbit IgG, HRP-linked	Bio-Rad	Cat# 170-6515, RRID:AB_11125142
Anti-mouse IgG HRP-linked	Bio-Rad	Cat# 170-6516, RRID:AB_11125547
Biological samples		
Tumor samples from patients with lung adenocarcinoma	University of Pennsylvania (IRB protocol # 805800).	N/A
Chemicals, peptides, and recombinant proteins		
EGF	R&D	P01133
HGF	R&D	P14210
PDGF	R&D	Q6FHE7
Gas6	R&D	NP_00081
Gefitinib	Tocris Bio-Techne Corporation	3000/10
LY294002	Tocris Bio-Techne Corporation	1130/5
Gö6983	Tocris Bio-Techne Corporation	2285/1
R428	VWR	1037624-75-1
SU11274	Selleckchem	S1080
PMA	LC Laboratories	P-1680
4’,6-Diamidino-2-phenylindole (DAPI)	Sigma	D9542
Rhodamine-phalloidin	ThermoFisher Scientific	R415
Critical commercial assays		
Rneasy kit	QIAGEN	74104
Taq-Man Reverse Transcription kit	QIAGEN	N8080234
Taqman Universal PCR Master Mix	ThermoFisher Scientific	4364340
Lipofectamine RNAi Max	Invitrogen	13778030

REAGENT or RESOURCE	SOURCE	IDENTIFIER
Fixable Viability Dye eFluor 450 staining	ThermoFisher Scientific	65-0863-14
Custom made Q-PCR array	ThermoFisher Scientific	Custom made
Experimental models: cell lines		
A549	ATCC	CCL-185
A549 KO cells	Kazanietz lab	Baker et al. (2020).
H358	ATCC	CRL-5807
H2009	ATCC	CRL-5911
H441	ATCC	HBT-174
H322	ATCC	CRL-5806
H1666	ATCC	CRL-5885
H1792	ATCC	CRL-5895
H1299	ATCC	CRL-5803
H1975	ATCC	CRL-5908
H2228	ATCC	CRL-5935
H2023	ATCC	CRL-5912
H1650	ATCC	CRL-5883
H3122	Mosse's lab (CHOP)	N/A
PC9	Sordella's lab (CSHL)	N/A
Oligonucleotides		
ABR siRNA	Dharmacon	J-008611-05-0002
ALS2 siRNA	Dharmacon	J-014168-09-0002
ARHGEF7 siRNA	Dharmacon	J-009616-05-0002
ARHGEF18 siRNA	Dharmacon	J-009654-05-0002
ARHGEF39 siRNA	Dharmacon	J-015006-05/06/07-0002
ECT2 siRNA	Dharmacon	J-006450-05-0002
FARP1 siRNA	Dharmacon	J-008519-06/07/08-0002
FARP2 siRNA	Dharmacon	J-009237-06-0002
PLEKHG2 siRNA	Dharmacon	J-023690-05-0002
P-REX1 siRNA	Dharmacon	J-010063-09-0002
RasGRF1 siRNA	Dharmacon	J-009323-05-0002
SPATA13 siRNA	Dharmacon	J-015469-09-0002
TIAM1 siRNA	Dharmacon	J-003932-05-0002
TIAM2 siRNA	Dharmacon	J-008434-09/10/11-0002
TRIO siRNA	Dharmacon	J-005047-05-0002
Vav2 siRNA	Dharmacon	J-005199-05-0002
NGEF siRNA	Dharmacon	J-009354-09-0002
PLEKHG3 siRNA	Dharmacon	J-022051-10-0002
ARHGEF16 siRNA	Dharmacon	J-010234-05-0002
ARHGEF6 siRNA	Dharmacon	J-010231-05-0002
ARHGEF4 siRNA	Dharmacon	J-008235-05-0002
VAV3 siRNA	Dharmacon	J-010178-06-0002
Shc1 siRNA	Dharmacon	J-018841-07-0002

REAGENT or RESOURCE	SOURCE	IDENTIFIER
Nck1 siRNA	Dharmacon	J-006354-06-0002
Grb2 siRNA	Dharmacon	J-019220-07-0002
Gab1 siRNA	Dharmacon	J-003553-05/06/07-0002
PTPN11 (SHP2) siRNA	Dharmacon	J-003947-09-0002
SOS1 siRNA	Dharmacon	J-005194-06-0002
AXL siRNA	Dharmacon	J-003104-10/11-0002
Recombinant DNA		
YFP-FARP1	Dr. Oliver Rock (MDC, Germany)	N/A
YFP-TIAM2	Dr. Oliver Rock (MDC, Germany)	Müller et al. (2020)
YFP-ARHGEF39	Dr. Oliver Rock (MDC, Germany)	Müller et al. (2020)
pFUGW-UbC-dCer3-PAK-dcpVen-Rac-WT (lentivirus)	Dr. Yi Wu (University of Connecticut Health Science Center)	Timmerman et al. (2015)
mCherry-Cortactin adenovirus	Garcia-Mata's lab	Goicoechea et al., 2017
Software and algorithms		
ImageJ	Available from NIH	https://imagej.nih.gov/ij/download.html
Sequence Detection System software version 1.7	Applied Biosystems	N/A
Rstudio version 1.4.1106	Rstudio	https://www.rstudio.com
Other		
GSE31210	Public access	https://www.ncbi.nlm.nih.gov/geo/query/acc.cgi?acc=GSE31210
CancerTools resource	http://genomics.cicbiogune.es/CANCERTOOL/	N/A